American Mineralogist, Volume 91, pages 229–246, 2006

PRESIDENTIAL ADDRESS†

Elastic properties of minerals and the influence of phase transitions

MICHAEL A. CARPENTER*

Department of Earth Sciences, University of Cambridge, Downing Street, Cambridge C2B 3EQ, U.K.

ABSTRACT

Elastic anomalies that accompany cation ordering and displacive phase transitions can be understood in terms of coupling between strain components and the driving order parameter in Landau free energy expansions. Non-convergent cation ordering in spinel, $MgAl_2O_4$, is accompanied by changes in individual elastic constants, shear modulus, and bulk modulus that vary linearly with the order parameter. Convergent cation ordering, such as Al/Si ordering in anorthite, is expected to give changes in elastic properties that scale with the square of the order parameter. The elastic anomalies that develop in association with displacive phase transitions show greater diversity, due to the additional influence of the order parameter susceptibility. These are illustrated for the cases of the proper ferroelastic transition at high pressure in stishovite and the improper ferroelastic transition in $SrTiO_3$ perovskite. Low temperature transitions in lawsonite show a more complex pattern of softening and stiffening that depends on coupling with both cation ordering and displacive processes. Variations of the spontaneous strain and elastic constants are indicative of the underlying thermodynamic mechanism for a phase transition. If any such transitions occur in minerals of the Earth's crust or mantle they should be identifiable from their distinctive influence on seismic velocities.

Keywords: Phase transitions, elastic constants, Landau theory, spinel, anorthite, stishovite, $SrTiO_3$, lawsonite

INTRODUCTION

Interest in seismic profiles through the Earth's crust and mantle is usually focused on the anomalies, which might be discontinuities or breaks in slope of velocity with depth. These are typically explained in terms of changes in bulk composition and/or mineral assemblage. In the case of olivine ↔ wadsleyite, changes in density and seismic velocity occur among olivine-bearing and wadsleyite-bearing assemblages across a narrow reaction zone in which both phases coexist. Pressure and temperature conditions for the reaction are known from experimental or computed phase diagrams, so that information on the temperature and bulk composition as a function of depth can be extracted (e.g., Agee 1998). The profile for a displacive phase transition would be quite different, however. For example, the $\alpha \leftrightarrow \beta$ transition in quartz has associated changes of single crystal elastic constants that start to develop at temperatures significantly away from the transition point itself (Fig. 1a, after Carpenter et al. 1998a). There is a density change of up to ~4% as a function of temperature (Fig. 1b), but this is accompanied by a total change in the bulk modulus of ~100%. In the vicinity of the transition point, the change in bulk modulus can even exceed this value. By way of contrast, the shear modulus barely changes and the result is a distinctive pattern of compressional and shear wave velocities (Fig. 1d). Mechie et al. (2004) claim to have identified this transition in a seismic profile from quartz-rich rocks in the Tibetan crust. Because the phase diagram is well-known and does not depend on what other phases might or might not be present, Mechie et al. were able to obtain a precise determination of the temperature at a depth of 18 km. There are several minerals, including silicate perovskites, clinopyroxenes, stishovite, and wüstite, which undergo phase transitions at high pressures and temperatures (e.g., Bina 1998; Prewitt and Downs 1998). It is well established that displacive transitions can give rise to a wide variety of elastic anomalies, which depend on the exact mechanism and thermodynamic character of the transition (Carpenter and Salje 1998, and many references therein). Therefore, the expectation must be that these too would give rise to quite distinctive, if not unique, patterns of seismic velocity variation. They might then convey precise temperatures for points on the geotherm within the mantle.

Geophysical considerations form only part of a wider interest in the elastic behavior of silicates and oxides. Elastic properties differ fundamentally from many other equilibrium properties in that they depend on the second derivative of free energy rather than the first derivative. In other words, they are related to the shape of the free energy potential and not simply to the location of minima. As a result, they are highly sensitive to any structural change that occurs in a crystal, to the extent that the comparison of values calculated from a model with values from experiments often provides a stringent test for the validity of the model. Elasticity is also an important factor in the development of ferroelectric and piezoelectric ceramics. Against this general background, the purpose of the present paper is to present a quantitative analysis of the influence on elastic properties of non-convergent cation ordering in spinel, convergent ordering in anorthite, displacive transitions in stishovite and $SrTiO_3$, and

* E-mail: mc43@esc.cam.ac.uk

† Paper presented at Geological Society of America Meeting in Denver, Colorado on November 9, 2004.

0003-004X/06/0203–229$05.00/DOI: 10.2138/am.2006.1979

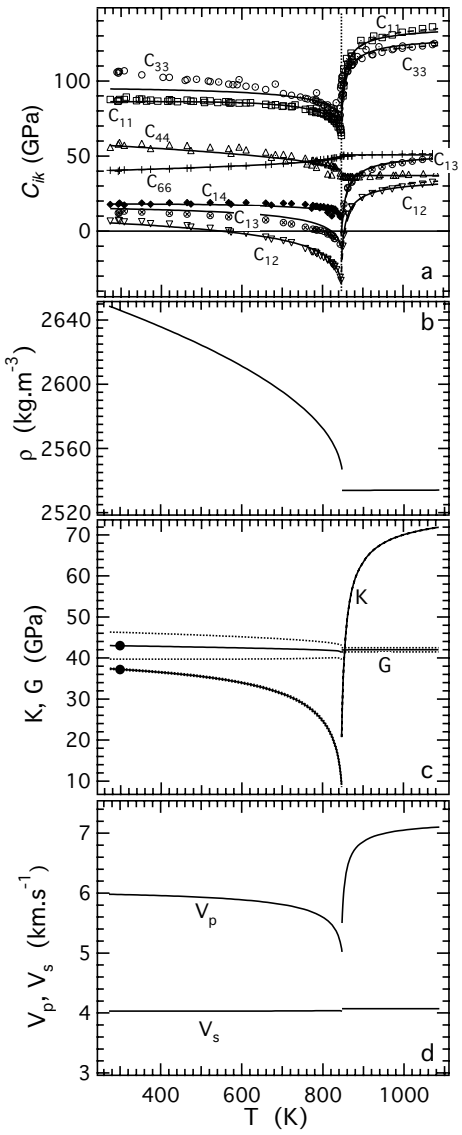

FIGURE 1. Changes in selected physical properties through the α ↔ β transition as a function of temperature in quartz. (**a**) Single-crystal elastic constants from the literature (individual symbols) are described by solutions to a Landau free energy expansion for α-quartz and by an expression for the effects of fluctuations in β-quartz (solid lines), after Carpenter et al. (1998a). (**b**) Density changes calculated from the lattice parameter variations given in Carpenter et al. (1998a). (**c**) Variations of the bulk and shear moduli of polycrystalline samples (solid lines) calculated using expressions for Voigt and Reuss limits (dotted lines) from Watt and Peselnik (1980) and the calculated single crystal elastic constants shown in **a**. Filled circles are bulk and shear moduli obtained for a polycrystalline quartz sample at ambient conditions (M.A. Carpenter and T.W. Darling, unpublished data). (**d**) Variation of P and S wave velocities, V_p and V_s, calculated using the Voigt/Reuss averages shown in **c** and the densities shown in **b**.

of combined proton ordering and displacive effects in lawsonite. $SrTiO_3$ is used as an analog for the possible behavior of silicate perovskites.

Variations in physical properties due to phase transitions in silicate minerals appear to conform closely to the precepts of Landau theory. In the case of quartz, the order parameter is related to a soft optic mode, which is responsible for the α ↔ β transition. Elastic softening below the transition temperature arises as a consequence of coupling among lattice strains and this driving order parameter. Softening in the stability field of the β form is due to a different mechanism, but the overall approach leads to close agreement between calculated and observed variations of the elastic constants (Fig. 1a). More generally, atomic displacements or changes in the degree of cation order are invariably accompanied by changes in lattice parameters, which are described formally as strains. The total free energy change, G, can be expressed as

$$G = G(Q) + G(Q, e_i) + \frac{1}{2}\sum_{i,k=1-6} C_{ik}^0 e_i e_k \quad (1)$$

where the first term describes energy changes due to the order parameter, Q, alone. The second term describes the energy due to coupling between the order parameter and strain, e_i (i = 1–6). The third term describes the work done against the elastic constants, C_{ik}^0, according to Hooke's law. (A superscript ^{0} is used to signify elastic constants that do not include the effects of the transition). Because the strains are coupled with the order parameter, atomic displacements and changes in order will modify both the strain state and the elastic constants. For phase transitions in general the critical issues are the constraints of symmetry on how a crystal deforms, the strength of coupling between the order parameter and strain and the timescale on which a change in strain state causes a change in the order parameter,

Strain/order parameter coupling terms in Equation 1 might have the form λeQ, λeQ^2, or λe^2Q^2, where the coefficient λ describes the strength of the coupling. In the case of displacive transitions, a small change in strain induces an effectively instantaneous change in the order parameter because the timescale for relaxations of Q is rapid in comparison with the timescale for changes in strain. The elastic constants then depend on second derivatives with respect to both Q and e, according to the well-known solution of Slonczewski and Thomas (1970),

$$C_{ik} = \frac{\partial^2 G}{\partial e_i \partial e_k} - \sum_{m,n} \frac{\partial^2 G}{\partial e_i \partial Q_m} \cdot \left(\frac{\partial^2 G}{\partial Q_m \partial Q_n} \right)^{-1} \cdot \frac{\partial^2 G}{\partial e_k \partial Q_n}. \quad (2)$$

For coupling of the form λeQ^2, an elastic constant of the low symmetry phase, C_{ik}, is thus softer than the equivalent elastic constant of the high symmetry phase, C_{ik}^0, by an amount $4\lambda^2 Q^2 \chi$, where χ [$=(\partial^2 G/\partial Q^2)^{-1}$] is the order parameter susceptibility. For cation ordering, an imposed strain should still produce a change in Q but the response time will be much slower due to the need for diffusion of atoms among crystallographic sites. This relaxation will not occur on the timescale of any normal elastic constant measurement, and coupling of the form λeQ or λeQ^2 does not contribute to any softening effects. Individual elastic constants are therefore derived from free energy expressions such as Equation 1 simply by taking $C_{ik} = \partial^2 G/\partial e_i \partial e_k$. Softening (or stiffening) will generally arise from coupling terms of the form $\lambda e_i e_k Q$ or $\lambda e_i e_k Q^2$, and there is no dependence on χ.

For both order/disorder and displacive effects the starting point for any quantitative analysis is the relationship between the order parameter and strain, as given explicitly in Landau

free energy expansions. For readers unfamiliar with this topic, convenient access points to the literature are perhaps Carpenter and Salje (1998) and Carpenter et al. (1998b).

Non-convergent ordering in spinel, $MgAl_2O_4$

Interdisciplinary research on spinels has been conducted in the context both of their stability in natural mineral assemblages at high pressures and temperatures and of their properties in oxide ceramics. One focus has been on the role of cation ordering in modifying thermodynamic properties and behavior. Non-convergent Mg/Al ordering in $MgAl_2O_4$, in particular, has been investigated using a wide variety of experimental techniques, including calorimetry (Navrotsky and Kleppa 1967; Navrotsky et al. 1986; Navrotsky 1986), ESR spectroscopy (Schmocker and Waldner 1976), NMR spectroscopy (Wood et al. 1986; Millard et al. 1992; Maekawa et al. 1997), Raman spectroscopy (Cynn et al. 1992, 1993; Van Minh and Yang 2004), X-ray diffraction at room temperature on quenched samples or in-situ at high temperatures (Yamanaka and Takéuchi 1983; Andreozzi et al. 2000; Carbonin et al. 2002), neutron diffraction at high temperatures and pressures (Peterson et al. 1991; Redfern et al. 1999; Pavese et al. 1999; Méducin et al. 2004), Resonant Ultrasound Spectroscopy (Cynn et al. 1993; Suzuki et al. 2000) and Brillouin scattering (Askarpour et al. 1993). Thermodynamic and structural models have also been developed (Navrotsky and Kleppa 1967; O'Neill and Navrotsky 1983; Sack and Ghiorso 1991; Della Giusta and Ottonello 1993; Carpenter and Salje 1994a; Hazen and Yang 1999), and modern computational methods have been applied to simulate the effects of pressure and temperature (Warren et al. 2000a, 2000b; Lavrentiev et al. 2003; Da Rocha and Thibaudeau 2003). Lattice parameter variations accompanying Mg/Al ordering are small, but the most recent studies appear to be settling on the view that disordering is associated with a decrease in volume and is therefore favored at high pressures (Andreozzi et al. 2000; Da Rocha and Thibaudeau 2003; Méducin et al. 2004). Direct measurements of elastic properties also suggest that there are small changes in the bulk and shear moduli (Cynn et al. 1993; Askarpour et al. 1993; Suzuki et al. 2000), but these have not been analyzed specifically in terms of an order/disorder model. Hazen and Yang (1999) proposed that increasing normal order would cause an increase in bulk modulus, while Lavrentiev et al. (2003) concluded that the bulk modulus would decrease. There appears to be very little discussion in the literature of the effect of ordering on the shear modulus of a polycrystalline sample.

A simple model for the influence of cation ordering in $MgAl_2O_4$ on strain and elastic properties can be developed from the Landau expansion given by Carpenter and Salje (1994a)

$$\begin{aligned} G = {} & hQ + \frac{1}{2}a(T - T_c)Q^2 + \frac{1}{3}bQ^3 + \ldots + \lambda_1 e_a Q + \lambda_2 e_a^2 Q + \ldots \\ & + \lambda_3\left(e_o^2 + e_t^2\right)Q + \ldots + \lambda_4\left(e_4^2 + e_5^2 + e_6^2\right)Q + \ldots \\ & + \frac{1}{6}\left(C_{11}^0 + 2C_{12}^0\right)e_a^2 + \frac{1}{4}\left(C_{11}^0 - C_{12}^0\right)\left(e_o^2 + e_t^2\right) \\ & + \frac{1}{2}C_{44}^0\left(e_4^2 + e_5^2 + e_6^2\right), \end{aligned} \tag{3}$$

where T is temperature and h, a, b are standard Landau coefficients. T_c is a temperature, which, in the context of non-convergent ordering processes, can be understood in terms of the strength of pairwise cation-cation interaction energies (Carpenter et al. 1994). Dots indicate that higher order terms in Q could be included if necessary, but will be considered to be negligibly small. The order parameter is related to the more commonly used inversion parameter, x, of spinels by

$$Q = -\frac{3}{2}x + 1 \tag{4}$$

(Carpenter and Salje 1994a). To express the symmetry of the strain/order parameter coupling correctly, the linear strains, e_1, e_2, and e_3, are given in their symmetry-adapted forms as

$$e_a = e_1 + e_2 + e_3 \tag{5}$$

$$e_o = e_1 - e_2 \tag{6}$$

$$e_t = \frac{1}{\sqrt{3}}\left(2e_3 - e_1 - e_2\right). \tag{7}$$

A more explicitly configurational form of the entropy term can be used if required, but this only affects the equilibrium evolution of Q and not its relationship with strain or the elastic constants. The most important feature of this expansion is that terms linear in Q are permitted because the ordering process does not cause a change in symmetry.

Variations of the strains are given by the usual equilibrium conditions $\partial G/\partial e_a = \partial G/\partial e_o = \partial G/\partial e_t = \partial G/\partial e_4 = 0$, from which it is easy to show that $e_o = e_t = e_4 = 0$ and

$$e_a = \frac{-\lambda_1 Q}{\frac{1}{3}\left(C_{11}^0 + 2C_{12}^0\right) + 2\lambda_2 Q}. \tag{8}$$

For $1/3\left(C_{11}^0 + 2C_{12}^0\right) >> 2\lambda_2 Q$, this reduces to

$$e_a = \frac{-\lambda_1 Q}{\frac{1}{3}\left(C_{11}^0 + 2C_{12}^0\right)}. \tag{9}$$

This linear relationship is consistent with the data of Andreozzi et al. (2000) for lattice parameters determined at room temperature (Fig. 2a). The linear strain is defined in the usual way (e.g., see Carpenter et al. 1998b) as $e_1 = (a - a_o)/a_o$, where a_o is the lattice parameter of a crystal with $Q = 0$ at the same temperature for which the lattice parameter a is specified. From Figure 2a, the total volume strain, e_a (= $3e_1$), for a change from $Q = 0$ to $Q = 1$ is 0.0060 ± 0.0003. This gives $\lambda_1 = -1.18 \pm 0.06$ GPa for $1/3(C_{11}^0 + 2C_{12}^0) = 196$ GPa (from Suzuki et al. 2000). The calculations of Da Rocha and Thibaudeau (2003) produced a similar volume strain, though with a slightly non-linear dependence on the degree of order (see their Figs. 4 and 5).

If a strain was induced by the application of hydrostatic pressure, the degree of order of a crystal of $MgAl_2O_4$ should change through the effect of the coupling term $\lambda_1 e_a Q$. This type of relaxation is kinetically unfavorable, however, and so cannot contribute to changes in the elastic constants. Changes in the bulk modulus therefore depend on the next higher order term, $\lambda_2 e^2{}_a Q$, and are given simply by

$$\frac{1}{3}\left(C_{11} + 2C_{12}\right) = \frac{\partial^2 G}{\partial e_a^2} = \frac{1}{3}\left(C_{11}^0 + 2C_{12}^0\right) + 2\lambda_2 Q. \tag{10}$$

The dependences of $(C_{11} - C_{12})$ and C_{44} on Q are given,

similarly, by

$$\frac{1}{2}(C_{11}-C_{12})=\frac{\partial^2 G}{\partial e_o^2}=\frac{\partial^2 G}{\partial e_t^2}=\frac{1}{2}\left(C_{11}^0-C_{12}^0\right)+2\lambda_3 Q \qquad (11)$$

$$C_{44}=\frac{\partial^2 G}{\partial e_4^2}=C_{44}^0+2\lambda_4 Q\,. \qquad (12)$$

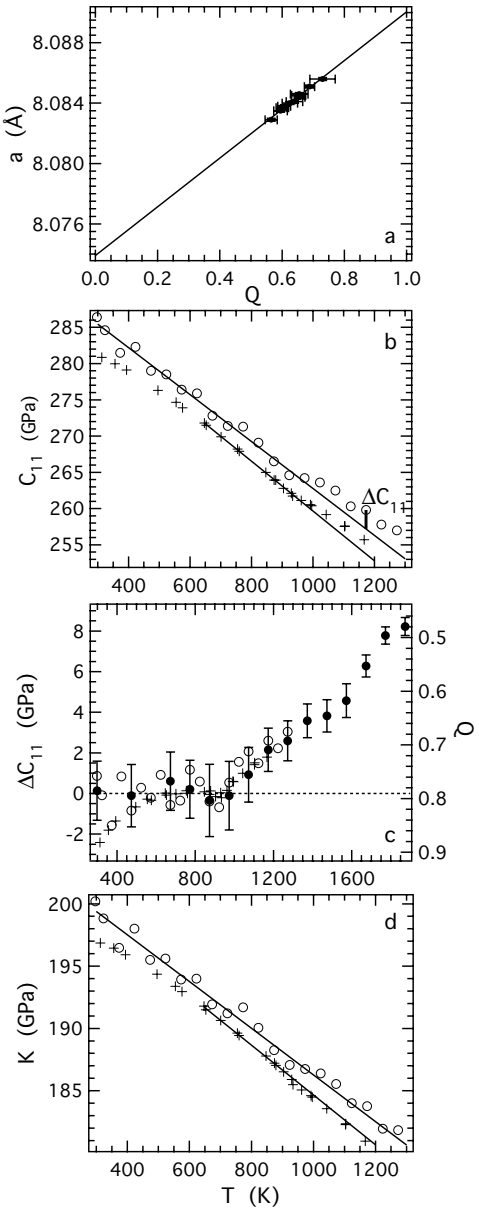

FIGURE 2. Strain and elastic constant changes due to Mg/Al ordering in $MgAl_2O_4$. Open circles are data from Askarpour et al. (1993); crosses are data from Suzuki et al. (2000). (**a**) Room-temperature data from Andreozzi et al. (2000) can be described by a straight line, $a = 8.0739 + 0.0161\,Q$. (**b**) A break in slope at ~925 K is interpreted as being due to kinetic effects such that changes in C_{11}, ΔC_{11}, at high temperatures are due to changes in the degree of order. (**c**) ΔC_{11} (open circles and crosses, left axis) from **b** varies linearly with Q (filled circles, right axis) from Redfern et al. (1999) (their ISIS neutron diffraction results). (**d**) Changes in bulk modulus associated with changes in Q above ~900 K are hardly greater than the scatter in the data.

From Equations 10 and 11, it follows that

$$C_{11}=C_{11}^0+\frac{1}{3}(6\lambda_2+8\lambda_3)Q \qquad (13)$$

$$C_{12}=C_{12}^0+\frac{1}{3}(6\lambda_2-4\lambda_3)Q\,. \qquad (14)$$

Askarpour et al. (1993) measured C_{11}, C_{12}, and C_{44} in-situ at high temperatures by Brillouin spectroscopy. Their data for C_{11} are reproduced in Figure 2b, showing a break in slope at ~925 K. Data for C_{11} obtained by Suzuki et al. (2000) using Resonant Ultrasound Spectroscopy show the same break in slope, though the absolute values are ~1.5% smaller (Fig. 2b). These elastic constants were measured under quite similar conditions of time and temperature to those used by Redfern et al. (1999) to collect neutron powder diffraction data. The break in slope of C_{11} coincides with the temperature above which Redfern et al. found that equilibrium order is achieved in-situ and below which the order parameter becomes fixed due to kinetic factors (see also Van Minh and Yang 2004). According to Equation 13 a change in Q should induce a linearly dependent change in C_{11}, ΔC_{11}. This can be tested by first assuming that Q remains constant below 925 K in all the experiments and then using changes at $T > 925$ K to calculate values for ΔC_{11} (Fig. 2b). A straight line therefore has been fit to the data for C_{11} from Askarpour et al. over the temperature range 297–923 K and from Suzuki et al. (2000) over the range ~650–900 K. Values of ΔC_{11}, calculated as the difference between observed values and the straight lines extrapolated to high temperatures, are plotted together with the order parameter values of Redfern et al. in Figure 2c. The axis for Q has been scaled to show that a linear relationship between ΔC_{11} and Q is indeed permitted by the data. From the relationships in Figure 2c, it is possible to extrapolate to $\Delta C_{11} = -26.1$ GPa for $Q = 0 \rightarrow Q = 1$. Similar analysis of the data of Askarpour et al. and Suzuki et al. for C_{12} gives $\Delta C_{12} = 10.3$ GPa for $Q = 0 \rightarrow Q = 1$. There is no detectable anomaly in C_{44}. Equations 12–14 then yield $\lambda_4 = 0$, $\lambda_2 = -0.9$, $\lambda_3 = -9.1$ GPa. The contribution of increased ordering to the bulk modulus can be given as $\Delta K = -1.8\,\Delta Q$ and to the Voigt/Reuss average of the shear modulus as $\Delta G \approx -12\,\Delta Q$ (at room temperature). Data for the adiabatic bulk modulus from Askarpour et al. and Suzuki et al. are reproduced in Figure 2d to show that the changes in order indeed have a negligible effect, though the latter perhaps signify that ordering actually causes a very small increase in K. Thus the main effect of increasing the degree of normal non-convergent ordering in $MgAl_2O_4$ is to lower the shear modulus. Equations 9 and 12–14 provide calibrations of this effect as linear functions of Q. Changes in the individual elastic constants, due to complete ordering from a fully disordered state, would be restricted to <10% (~9% for C_{11} and ~7% for C_{12}). These changes in elastic constants are accompanied by small increases in volume, which are also expected to be linear in Q.

CONVERGENT ORDERING IN ANORTHITE

There are a few studies of the spontaneous strains which accompany cation ordering transitions in specific minerals. These include, for example, Al/Si ordering in K-feldspar (Carpenter and Salje 1994b), anorthite (Carpenter et al. 1990), and cordierite (Putnis et al. 1987), Fe/Ti ordering in iron-titanium

oxides (Harrison et al. 2000) and cation/vacancy ordering in staurolite (Hawthorne et al. 1993). Systematic information on elastic constants is sparse, however. There are data for the bulk modulus of anorthite crystals with different degrees of order due to Hackwell and Angel (1992) and Angel (1992, 1994), however, which at least allow an illustration of how the elastic effects associated with the $C\bar{1} \leftrightarrow I\bar{1}$ transition due to Al/Si ordering might be analyzed. The relevant strain/order parameter coupling terms in the excess free energy can be written as $\lambda_1 V_s Q^2 + \lambda_2 V_s^2 Q^2 + \frac{1}{2}(K^0 V_s^2)$, where V_s is the volume strain of the ordered $I\bar{1}$ structure, with respect to the disordered $C\bar{1}$ structure, and K^0 is the bulk modulus of the $C\bar{1}$ structure. The order parameter, Q, is given by the degree of Al/Si order as extracted from average cation-oxygen bond lengths at the tetrahedral sites (Angel et al. 1990; Carpenter et al. 1990).

The relationship between V_s and Q is obtained from the equilibrium condition, $\partial G/\partial V_s = 0$, which gives

$$V_s = \frac{-\lambda_1 Q^2}{K^0} \tag{15}$$

for the condition $K^o >> 2\lambda_2 Q^2$. As with ordering in spinel, Q does not immediately change when a stress is applied, so that coupling of the form $\lambda_1 V_s Q^2$ does not contribute to any elastic softening. Instead, the bulk modulus is expected to vary according to

$$K = \frac{\partial^2 G}{\partial V_s^2} = K^0 + 2\lambda_2 Q^2. \tag{16}$$

Analysis of experimental data for the volume strain and bulk modulus is complicated by the fact that anorthite has $P\bar{1}$ symmetry at room temperature due to a displacive ($I\bar{1} \leftrightarrow P\bar{1}$) transition at ~510 K, 1 bar (Redfern and Salje 1987, 1992; Ghose et al. 1988; Smith and Brown 1988; Van Tendeloo et al. 1989; Redfern et al. 1988; Redfern 1992, and many references therein) and between 2.5 and 5 GPa at room temperature (Angel 1988; Angel et al. 1988, 1989). Evolution of the order parameter for this transition is sensitive to the degree of Al/Si order (Salje 1987; Redfern et al. 1988; Angel et al. 1989; Redfern 1992; Angel 1992), with the result that the volume behavior depends on two interdependent order parameters. There are sufficient data for An-rich samples in the plagioclase solid solution at least to show that increasing Al/Si order causes the volume to decrease very slightly (Carpenter et al. 1985; Angel et al. 1990; Angel 2004) and, hence, that V_s is negative. The coefficient λ_1 in Equation 15 is thus expected to be small and positive. Data for the bulk modulus as a function of Al/Si order have been extracted from measurements of lattice parameters as a function of pressure at room temperature by Hackwell and Angel (1992) and Angel (1992). Values of K_o listed by Angel (1994) for both $I\bar{1}$ and $P\bar{1}$ crystals were obtained by fitting a Murnaghan equation of state to the volume data for each of the structural states at high pressures, keeping $K' = 4$. These are plotted against Q^2 in Figure 3. (Note that K_o refers to the bulk modulus at zero pressure in the Murnaghan equation of state and should not be confused with K^o in Equations 15 and 16, which signifies the bulk modulus of Al/Si disordered, $C\bar{1}$, crystals). Taken at face value, K_o appears to conform to the expected $K \propto Q^2$ dependence (Eq. 16), with $\lambda_2 \approx 21$ GPa for crystals with $P\bar{1}$ symmetry and ≈ 99 GPa for crystals with $I\bar{1}$ symmetry (Fig. 3). A definitive interpretation will need to take account of the influence of the displacive transition, however. In the $I\bar{1}$ stability field, the bulk modulus might soften due to the effects of thermal fluctuations as the transition point is approached. In the $P\bar{1}$ stability field the bulk modulus will vary strongly due to the same strain/order parameter coupling mechanism as in quartz. Moreover, the displacive transition is strongly first order in highly ordered crystals but changes toward second order character in more disordered samples (Angel 1992). These effects will give a quite different pressure dependence for K and it is not appropriate to use the data for K_o obtained with $K' = 4$ in the uncritical way represented by Figure 3. Extracting bulk modulus information as a function of pressure in these circumstances is a difficult problem (Tröster et al. 2002). In particular, the bulk modulus for $P\bar{1}$ crystals should be smaller than the bulk modulus for $I\bar{1}$ crystals at any given pressure if the $I\bar{1} \leftrightarrow P\bar{1}$ transition is a classical displacive transition.

There are no data for the shear modulus as a function of Al/Si order but, as the total scalar strain due to the $C\bar{1} \leftrightarrow I\bar{1}$ transition is observed to vary with Q^2 (Carpenter et al. 1990) and all the individual strains have the symmetry of the identity representation (giving $e_i \propto Q^2$ for i = 1–6), it seems likely that the shear modulus will also vary linearly with Q^2.

Elastic softening due to displacive transitions

The example of a co-elastic transition, $\alpha \leftrightarrow \beta$ quartz, has already been given (Fig. 1). In this section, examples of proper ferroelastic and improper ferroelastic transitions are reviewed. As well as having potential implications in a geophysical context, they illustrate two further patterns of elastic constant anomalies that can occur in minerals as a consequence of strain/order parameter coupling.

Proper ferroelastic transition in stishovite, SiO_2

A $P4_2/mnm \leftrightarrow Pnnm$ phase transition occurs at high pressures in several AO_2 compounds that have the same structure as

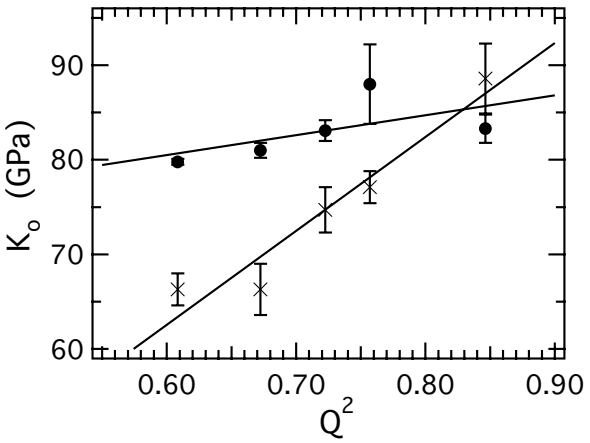

Figure 3. Variations of the zero pressure bulk modulus at room temperature and zero pressure for anorthite crystals with different degrees of Al/Si order are consistent with $K \propto Q^2$. Data from Hackwell and Angel (1992) and Angel (1992), as listed in Angel (1994), determined by fitting a Murnaghan equation of state with $K' = 4$ to single crystal diffraction data. Filled circles represent $P\bar{1}$ structures; crosses represent $I\bar{1}$ structures.

rutile. These include stishovite (Cohen 1994; Hemley et al. 1994; Kingma et al. 1995; Lee and Gonze 1995, 1997; Dubrovinsky and Belonoshko 1996; Karki et al. 1997a, 1997b; Andrault et al. 1998, 2003; Teter et al. 1998; Carpenter et al. 2000; Hemley et al. 2000; Shieh et al. 2002; Ono et al. 2002a; Tsuchiya et al. 2004), GeO_2 (Haines et al. 1998, 2000; Lodziana et al. 2001; Ono et al. 2002b), SnO_2 (Haines and Léger 1997; Parlinski and Kawazoe 2000; Hellwig et al. 2003), RuO_2 (Haines and Léger 1993; Haines et al. 1997), PbO_2 (Haines et al. 1996), and MnO_2 (Haines et al. 1995). The same transition also occurs in a number of halides, including $CaBr_2$ and $CaCl_2$ at high temperatures (Bärnighausen et al. 1984; Raptis et al. 1989; Unruh 1993; Hahn and Unruh 1991; Kennedy and Howard 2004) and MgF_2 at high pressures (Haines et al. 2001). The mechanism involves softening of A_g and B_{1g} optic modes of the orthorhombic and tetragonal structures, respectively. Data for the frequency variation of these modes in stishovite are reproduced from Kingma et al. (1995) in Figure 4 to show the classic relationship for a proper ferroelastic transition driven by a zone center soft optic mode (see also Haines et al. 1998, Hellwig et al. 2003, and Unruh 1993 for the same behavior in GeO_2, SnO_2, and $CaCl_2$). The critical pressure, P_c, at which the B_{1g} mode would go to zero frequency is 102.3 GPa, whereas the transition occurs at P_c^* = 51.6 GPa (Fig. 4) due to bilinear coupling of the order parameter with the symmetry breaking strain, e_1–e_2.

Strain and elastic constant variations through the transition in stishovite have been obtained from a Landau expansion (from Carpenter et al. 2000)

$$\begin{aligned} G = {} & \frac{1}{2}a(P-P_c)Q^2 + \frac{1}{4}bQ^4 + \lambda_1(e_1+e_2)Q^2 + \lambda_2(e_1-e_2)Q \\ & + \lambda_3 e_3 Q^2 + \lambda_4\left(e_4^2 - e_5^2\right)Q + \lambda_6 e_6^2 Q^2 \\ & + \frac{1}{4}\left(C_{11}^0 + C_{12}^0\right)(e_1+e_2)^2 + \frac{1}{4}\left(C_{11}^0 - C_{12}^0\right) \\ & (e_1-e_2)^2 + C_{13}^0(e_1+e_2)e_3 + \frac{1}{2}C_{33}^0 e_3^2 \\ & + \frac{1}{2}C_{44}^0\left(e_4^2+e_5^2\right) + \frac{1}{2}C_{66}^0 e_6^2. \end{aligned} \tag{17}$$

Spontaneous strains evolve with Q according to

$$(e_1-e_2) = \left(\frac{-\lambda_2}{\frac{1}{2}\left[C_{11}^0 - C_{12}^0\right]}\right)Q \tag{18}$$

$$e_3 = \left(\frac{2\lambda_1 C_{33}^0 - \lambda_3\left[C_{11}^0 + C_{12}^0\right]}{C_{33}^0\left[C_{11}^0 + C_{12}^0\right] - 2C_{13}^{02}}\right)Q^2 \tag{19}$$

$$(e_1+e_2) = \left(\frac{2\lambda_3 C_{13}^0 - 2\lambda_1 C_{33}^0}{C_{33}^0\left[C_{11}^0 + C_{12}^0\right] - 2C_{13}^{02}}\right)Q^2. \tag{20}$$

Note that the variations of e_3 and e_1+e_2 were given incorrectly in Carpenter et al. (2000). In renormalized form, Equation 17 becomes

$$G = \frac{1}{2}a\left(P - P_c^*\right)Q^2 + \frac{1}{4}b^*Q^4 \tag{21}$$

where the transition pressure is given by

$$P_c^* = P_c + \frac{\lambda_2^2}{a\frac{1}{2}\left(C_{11}^0 - C_{12}^0\right)} \tag{22}$$

and the renormalized fourth order coefficient is

$$b^* = b - 2\left[\frac{\lambda_3^2\left(C_{11}^0 + C_{12}^0\right) + 2\lambda_1^2 C_{33}^0 - 4\lambda_1\lambda_3 C_{13}^0}{\left(C_{11}^0 + C_{12}^0\right)C_{33}^0 - 2C_{13}^{0\,2}}\right]. \tag{23}$$

The order parameter evolves according to

$$Q^2 = \frac{a}{b^*}\left(P_c^* - P\right). \tag{24}$$

Lattice parameter variations as a function of pressure are shown in Figures 5a–5c. The strains derived from these, $(e_1–e_2) = (a - b)/a_o$, $(e_1+e_2) = (a + b - 2a_o)/a_o$, $e_3 = (c - c_o)/c_o$, where a_o and c_o are tetragonal parameters extrapolated into the stability field of the orthorhombic structure, are dominated by the symmetry-breaking shear strain, $(e_1–e_2)$. This varies as $(e_1–e_2)^2 \propto P$, showing that the transition is second order in character in stishovite (Fig. 5d) as well as in SnO_2 (Haines and Léger 1997), GeO_2 (Haines et al. 2000), MnO_2 (Haines et al. 1995), RuO_2 (Haines and Léger 1993), and MgF_2 (Haines et al. 2001). In $CaBr_2$, this strain evolves according to the solution for a 246 Landau potential (Kennedy and Howard 2004). The non-symmetry breaking strains, (e_1+e_2) and e_3, are much smaller and more difficult to determine accurately because of the need to adopt a non-linear extrapolation for a_o and c_o. The pattern for GeO_2 (Haines et al. 2000), $CaCl_2$ (Unruh 1993), and $CaBr_2$ (Kennedy and Howard 2004) is a reduction of the c dimension in the orthorhombic structure (e_3 negative) and a small reduction in volume (V_s negative). The data of Kennedy and Howard (2004) show that $(e_1 + e_2)$ is positive for $CaBr_2$. On the other hand, e_3 is positive and $(e_1 + e_2)$ negative in RuO_2 (see Fig. 3 of Haines and Léger 1993). The most recent determination of Andrault et al. (2003) is that V_s for stishovite is negative. These authors used a linear extrapolation for c_o, however, which gives positive values of e_3 and results which are incompatible with the requirement that $V_s = e_1 + e_2 + e_3$ for small strains. For present purposes the analog behavior of GeO_2 is taken as

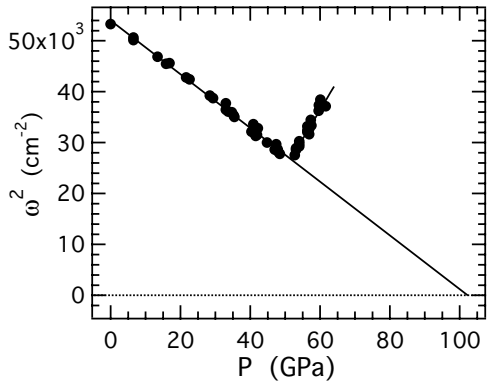

FIGURE 4. ω^2 for the B_{1g} soft optic mode of the tetragonal structure of stishovite extrapolates to zero at P_c = 102.3 GPa while the tetragonal ↔ orthorhombic transition occurs at P_c^* = 51.6 GPa (after Carpenter et al. 2000; data of Kingma et al. 1995).

providing the best evidence that e_3 for stishovite is negative. Values of λ_1 and λ_3 and, hence, of $b^* - b$ (Eq. 23), have been redetermined using the constraints that $b/b^* = 1.135$ from the ratio of slopes of the square of the soft mode frequencies as $P \rightarrow P_c^*$ from Carpenter et al. (2000) and $V_s \approx -0.003$ at 100 GPa from Andrault et al. (2003). The variations of a_o, c_o, and V_o are shown in Figures 5a–5c and the revised set of Landau parameters is listed in Table 1.

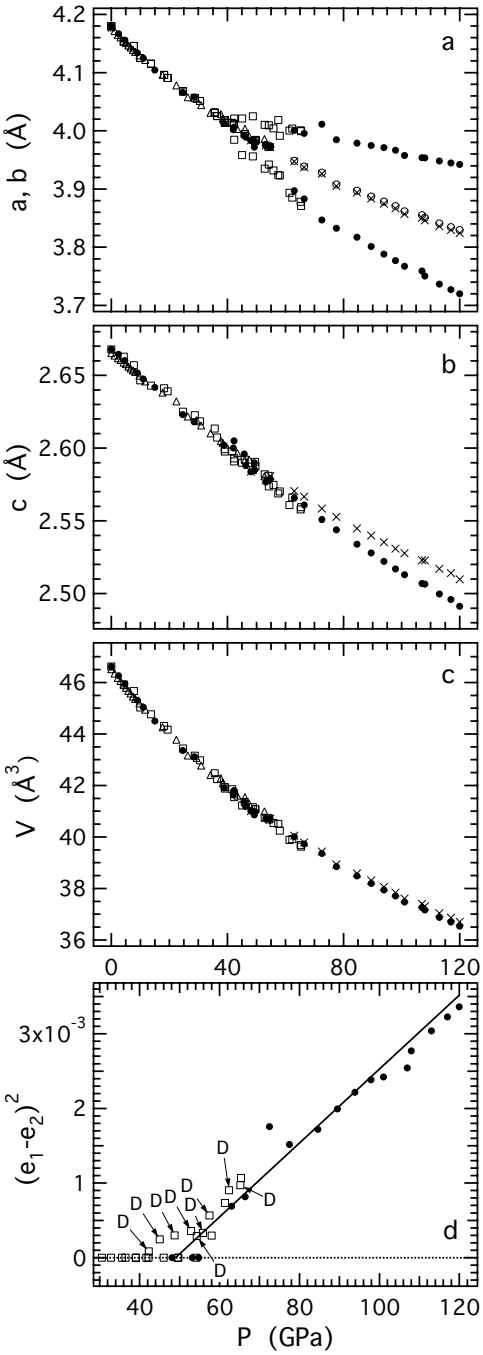

FIGURE 5. (**a**–**c**) Lattice parameter variations through the tetragonal ↔ orthorhombic transition in stishovite. Filled circles = Ross et al. 1990; Hemley et al. 1994; Andrault et al. 1998. Open squares = Mao et al. (1994). Open triangles = Andrault et al. (2003). Open circles are values of a_o defined by $a_o = (a \times b)^{0.5}$. Crosses are values of a, c_o, V_o obtained using experimental values of orthorhombic sitshovite and strains determined for $\lambda_1 = 1$, $\lambda_3 = 24$ GPa. (**d**) Variation of the square of the symmetry breaking strain with pressure (after Carpenter et al. 2000). D designates measurements of the orthorhombic phase made during decompression.

Elastic constant variations are obtained by applying Equation 2 to the full Landau expansion (Eq. 17). $(C_{11} - C_{12})$ should go to zero as the transition point is approached from above or below according to

$$(C_{11} - C_{12}) = (C_{11}^0 - C_{12}^0)\left(\frac{P - P_c^*}{P - P_c}\right) \quad (25)$$

while other elastic constants show the effects of the transition only as anomalies in the stability field of the orthorhombic structure. For example, $(C_{11} + C_{12})$ and C_{33} are expected to follow

$$(C_{11} + C_{12}) = (C_{11}^0 + C_{12}^0) - (8\lambda_1^2 Q^2 + 4\lambda_1\lambda_2 Q)\chi \quad (26)$$

$$C_{33} = C_{33}^0 - 4\lambda_3^2 Q^2 \chi . \quad (27)$$

Elastic constant variations, calculated using these expressions and the revised set of parameters listed in Table 1, are shown in Figure 6a (after Carpenter et al. 2000). Bulk and shear moduli of a polycrystalline sample (Voigt/Reuss averages using the expressions given by Watt 1979) are shown in Figure 6b. Values of the velocities of compressional and shear waves calculated from these are shown in Figure 6c. Due to the fact that a small negative volume strain has been included in the fitting of strain parameters, there is now a small discontinuity in the bulk modulus at the transition point (Fig. 6b). The bulk elastic properties are dominated by the influence of $(C_{11} - C_{12})$ softening, which extends to many GPa away from the transition point.

Ono et al. (2002a) have provided the first experimental determination of the temperature dependence of the tetragonal ↔ orthorhombic transition. They gave a positive slope of 0.012 ± 0.005 GPa/K, which compares with 0.0086 ± 0.0024 GPa/K for the same transition in GeO_2 (Ono et al. 2002b). Calculated slopes are 0.004 GPa/K (Kingma et al. 1995) and 0.006 GPa/K (Tsuchiya et al. 2004). These can be incorporated into the Landau description by adding a term in $\frac{1}{2}[a_T(T - T_c)Q^2]$ to Equations 17 and 21, where T_c is room temperature (295 K). Combining the terms in Q^2 then gives the second order transition as occurring when

$$a(P - P_c^*) + a_T(T - T_c) = 0 \quad (28)$$

TABLE 1. Values of parameters used to calculate the elastic constants as a function of pressure through the phase transition in stishovite

$C_{11}^0 = 578 + 5.38\,P$	$P_c^* = 49.0$
$C_{33}^0 = 776 + 4.94\,P$	$P_c - P_c^* = 50.7$
$C_{12}^0 = 86 + 5.38\,P$	$\lambda_1 = 1$
$C_{13}^0 = 191 + 2.72\,P$	$\lambda_2 = 24.62$
$C_{11}^0 - C_{12}^0 = 492$	$\lambda_3 = 24$
$C_{44}^0 = 252 + 1.88\,P$	$a = -0.04856$
$C_{66}^0 = 323 + 3.10\,P$	$b = 10.98$

Note: All values are given in units of GPa except for a, which is dimensionless.

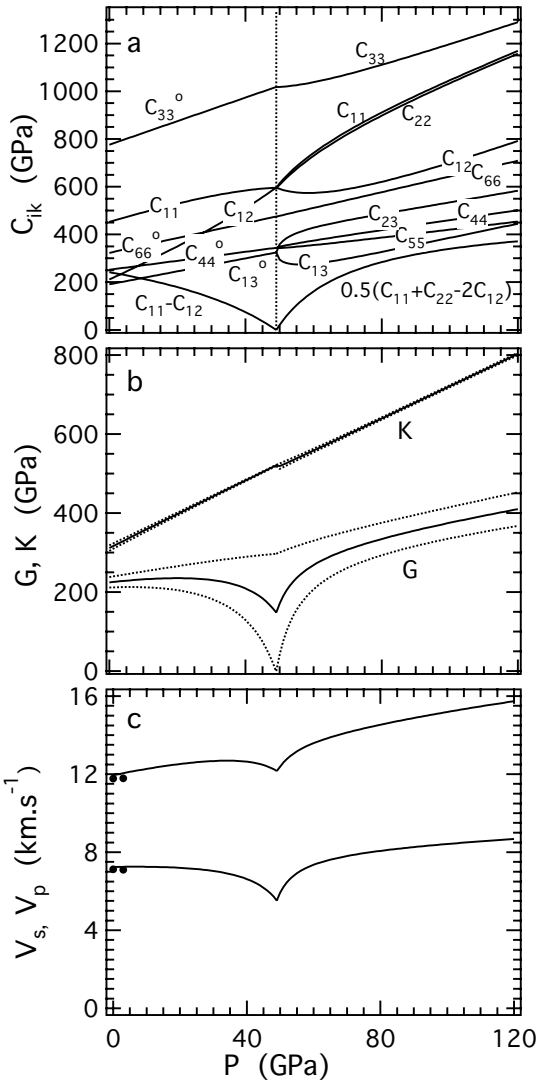

FIGURE 6. (**a**) Variation of elastic constants through the tetragonal ↔ orthorhombic transition in stishovite, based on expressions given in Carpenter et al. (2000) and the parameters listed in Table 1. (**b**) Bulk and shear moduli calculated as the average of Voigt and Reuss limits for a polycrystalline sample. Dotted lines represent Voigt and Reuss limits. (**c**) Calculated values of P (top) and S (lower) wave velocities through a polycrystalline sample. Filled circles indicate experimental values obtained by Li et al. (1996) at room pressure and 3 GPa.

Taking the *PT* slope of Ono et al. (2002a) and the value of P_c^* = 49 GPa from Carpenter et al. (2000), the transition pressure at 1295 K would be 64.5 ± 6.5 GPa. This gives a_T = 0.00075 ± 0.00032 GPa/K (≈ 9 ± 4 J/(mol·K). Adding temperature in this way allows values of the order parameter, the order parameter susceptibility and changes in the elastic constants to be calculated for simultaneous high pressures and temperatures, assuming that the Landau coefficients are not themselves temperature-dependent.

Interest in the ferroelastic transition in stishovite has been stimulated substantially by the possibility that a silica phase could be present in the lower mantle (see, for example, discussions and references in Carpenter et al. 2000; Ono et al. 2002a; Tsuchiya et al. 2004). Due to the phase transition, the shear modulus of stishovite will be much softer at these conditions than a simple extrapolation of the properties of tetragonal stishovite from ambient conditions would imply. While most (but not all) of the anomalies in individual elastic constants are reasonably well constrained by the input of data from strain and spectroscopic measurements, the pressure dependence of the bare elastic constants is taken from only one set of calculated values (Karki et al. 1997a). Recent experimental data of Shieh et al. (2002) suggest that C_{11}^0 and C_{12}^0 increase with pressure to a lesser extent than the calculations suggest. This is also consistent with the smaller pressure dependence of V_p implied by the two data points of Li et al. (1996) shown in Figure 6c. More important, in terms of real uncertainties for the absolute values of the shear modulus of polycrystalline orthorhombic stishovite, is the unknown influence of ferroelastic twins. Such twins can contribute to substantial softening beyond what is expected from the standard strain/order parameter coupling model (Kityk et al. 2000a, 2000b; Harrison and Redfern 2002; Harrison et al. 2003, 2004a, 2004b, 2004c). This effect, which also causes substantial attenuation, has not yet been characterized for the $P4_2/mnm \leftrightarrow Pnnm$ transition in AB_2 compounds. Finally, Cordier et al. (2004) have shown that additional elastic anisotropy caused by the phase transition would contribute to the development of crystal preferred orientations in polycrystalline samples subjected to non-hydrostatic stress. Texturing of this type would give rise to a strongly anisotropic seismic signature.

IMPROPER FERROELASTIC TRANSITION IN $SrTiO_3$ PEROVSKITE

Improper ferroelastic transitions due to octahedral tilting are common in perovskites. The stable form of (Mg,Fe)SiO_3 perovskite in the mantle is generally considered to be orthorhombic, with *Pnma* symmetry (Wentzcovitch et al. 1993; Stixrude and Cohen 1993; Fiquet et al. 1998; Ono et al. 2004a, and references therein). On the other hand, the current view of $CaSiO_3$ perovskite appears to be that it is tetragonal at ambient conditions, but could undergo a cubic ↔ tetragonal transition at *PT* conditions corresponding to those of the lower mantle (Stixrude et al. 1996; Ono et al. 2004b; Kurashina et al. 2004; Caracas et al. 2005). Tilting transitions among any of the possible polymorphs of $MgSiO_3$ or $CaSiO_3$ would certainly cause significant changes in their bulk elastic properties, but no data yet exist for these owing to the difficulty of measuring elastic constants at high pressures and temperatures. On the other hand there are abundant data for the analogous $Pm\bar{3}m \leftrightarrow I4/mcm$ transition in $SrTiO_3$, and these have recently been used to develop a quantitative model of elastic anomalies that accompany this transition (Carpenter, in preparation). Key features of the elastic behavior are reviewed here.

Octahedral tilting transitions from the cubic parent structure to *I*4/*mcm*, *Imma*, or $R\bar{3}c$ structures are expected to occur according to a Landau potential (to sixth order in *Q*)

$$
\begin{aligned}
G = {} & \frac{1}{2}a\Theta_s\left(\coth\left(\frac{\Theta_s}{T}\right)-\coth\left(\frac{\Theta_s}{T_c}\right)\right)\left(q_1^2+q_2^2+q_3^2\right)\\
& +\frac{1}{4}b\left(q_1^2+q_2^2+q_3^2\right)^2+\frac{1}{4}b'\left(q_1^4+q_2^4+q_3^4\right)\\
& +\frac{1}{6}c\left(q_1^2+q_2^2+q_3^2\right)^3+\frac{1}{6}c'\left(q_1q_2q_3\right)^2\\
& +\frac{1}{6}c''\left(q_1^2+q_2^2+q_3^2\right)\left(q_1^4+q_2^4+q_3^4\right)\\
& +\lambda_1 e_a\left(q_1^2+q_2^2+q_3^2\right)\\
& +\lambda_2\left[\sqrt{3}e_o\left(q_2^2-q_3^2\right)+e_t\left(2q_1^2-q_2^2-q_3^2\right)\right]\\
& +\lambda_3\left(e_4q_1q_3+e_5q_1q_2+e_6q_2q_3\right)\\
& +\frac{1}{4}\left(C_{11}^0-C_{12}^0\right)\left(e_o^2+e_t^2\right)+\frac{1}{6}\left(C_{11}^0+2C_{12}^0\right)e_a^2\\
& +\frac{1}{2}C_{44}^0\left(e_4^2+e_5^2+e_6^2\right).
\end{aligned}
\tag{29}
$$

Saturation of the order parameter components at low temperatures is described by the coth term, with Θ_s as the saturation temperature (Salje et al. 1991a, 1991b). The *I*4/*mcm* structure has $q_1 \neq 0$, $q_2 = q_3 = 0$ and symmetry-breaking strains which vary as

$$e_a = \frac{-\lambda_1 q_1^2}{\frac{1}{3}\left(C_{11}^0+2C_{12}^0\right)} \tag{30}$$

$$e_t = \frac{-2\lambda_2 q_1^2}{\frac{1}{2}\left(C_{11}^0-C_{12}^0\right)}. \tag{31}$$

The other strains, e_o, e_4, e_5, e_6, are all zero in the *I*4/*mcm* structure. In its renormalized form for the $Pm\bar{3}m \leftrightarrow I4/mcm$ transition, Equation 29 becomes

$$
\begin{aligned}
G = {} & \frac{1}{2}a\Theta_s\left(\coth\left(\frac{\Theta_s}{T}\right)-\coth\left(\frac{\Theta_s}{T_c}\right)\right)q_1^2\\
& +\frac{1}{4}\left(b^*+b'^*\right)q_1^4+\frac{1}{6}\left(c+c''\right)q_1^6
\end{aligned}
\tag{32}
$$

where

$$b^* = b-\frac{\lambda_3^2}{C_{44}^0}-\frac{2\lambda_1^2}{\frac{1}{3}\left(C_{11}^0+2C_{12}^0\right)}+\frac{4\lambda_2^2}{\frac{1}{2}\left(C_{11}^0-C_{12}^0\right)} \tag{33}$$

$$b'^* = b'+\frac{\lambda_3^2}{C_{44}^0}-\frac{12\lambda_2^2}{\frac{1}{2}\left(C_{11}^0-C_{12}^0\right)}. \tag{34}$$

Equation 32 is a standard Landau 246 potential for which the solution is

$$q_1^2 = \frac{-\left(b^*+b'^*\right)+\sqrt{\left(b^*+b'^*\right)^2+4a\left(c+c''\right)\Theta_s\left(\coth\left(\frac{\Theta_s}{T_c}\right)-\coth\left(\frac{\Theta_s}{T}\right)\right)}}{2\left(c+c''\right)}. \tag{35}$$

Dilatation data of Liu et al. (1997) have been combined with lattice parameter data of Okazaki and Kawaminami (1973) (with some scaling to give close overlap) to give the pattern of lattice parameter variations shown in Figure 7a. The reference parameter of the cubic phase, a_o, was fit with an expression of the form

$$a_o = a_c + a_s\Theta_{sa}\coth\left(\frac{\Theta_{sa}}{T}\right) \tag{36}$$

to account for the normal effects of thermal expansion as $T \rightarrow 0$ K (e.g., Meyer et al. 2000, 2001). Note that Θ_{sa} is the saturation temperature for thermal expansion and is unrelated to the order parameter saturation temperature, Θ_s. Variations of the tetragonal strain, e_t, and the volume strain, e_a, extracted from these data are shown in Figure 7b. To this has been added the 246 solution for q_1^2 from Hayward and Salje (1999) which provides a good representation of the variation of e_t. Absolute values of the volume strain are highly sensitive to the choice of baseline, a_o, but, even so, the variation of e_a does not vary linearly with q_1^2. This is a not uncommon feature of phase transitions in perovskites (Carpenter et al. 1998b) and implies either that the coupling coefficient λ_1 is temperature-dependent or that higher order terms, such as $\lambda e_a q_1^4$, contribute to the excess free energy for the transition.

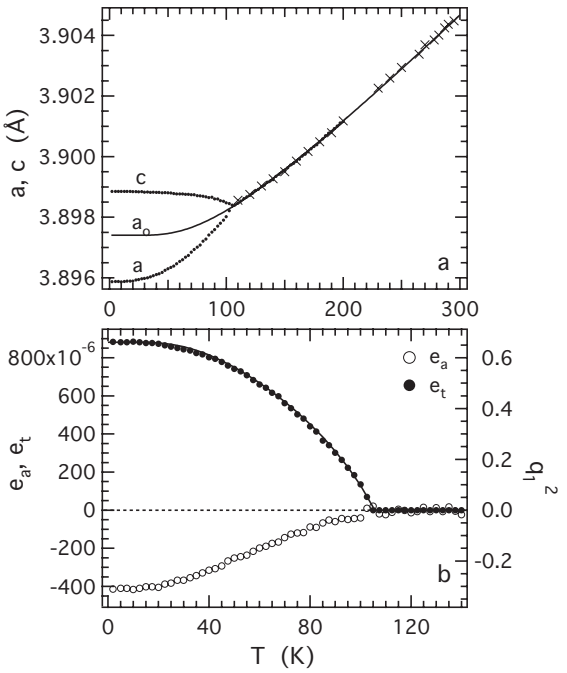

FIGURE 7. (**a**) Lattice parameter variations through the cubic ↔ tetragonal transition in $SrTiO_3$. Data for cubic $SrTiO_3$ up to 300 K (crosses) are from Okazaki and Kawaminami (1973). Data for cubic and tetragonal $SrTiO_3$ (dots) were extracted from Liu et al. (1997). The two data sets were scaled to produce the close overlap. A solid line defines the reference parameter, a_o, as given by fitting Equation 36 to data above T_c. (**b**) The tetragonal strain (e_t left axis) calculated from the data in **a** scales linearly with the solution for q_1^2 (solid line, right axis) from Hayward and Salje (1999). The volume strain (e_a, left axis) does not.

Expressions for elastic constant variations through the cubic ↔ tetragonal transition in $SrTiO_3$ were first derived by Slonczewski and Thomas (1970) and have been considered frequently in the literature (Rehwald 1970, 1971; Lüthi and Moran 1970; Fossheim and Berre 1972; Bulou et al. 1992; Kityk et al. 2000a). For example, the forms of C_{11} and C_{44} derived from Equation 29

are (from Carpenter, in preparation)

$$C_{11} = C_{22} = C_{11}^0 - \left(2\lambda_1 - \frac{4}{\sqrt{3}}\lambda_2\right)^2 \chi_1 q_1^2 \quad (37)$$

$$C_{44} = C_{55} = C_{44}^0 - \lambda_3^2 \chi_3 q_1^2 \quad (38)$$

where

$$\chi_1^{-1} = \frac{\partial^2 G}{\partial q_1^2} = 2\left(b + b'\right)q_1^2 + 4\left(c + c''\right)q_1^4 \quad (39)$$

$$\chi_3^{-1} = \frac{\partial^2 G}{\partial q_3^2} = \left[\frac{12\lambda_2^2}{\frac{1}{2}\left(C_{11}^0 - C_{12}^0\right)} - b'\right]q_1^2 - \frac{2}{3}c'' q_1^4. \quad (40)$$

Values for all the Landau coefficients in Equation 29 have been taken from Hayward and Salje (1999) or extracted from analysis of the strains. Variations of the individual elastic constants have then been calculated and compared with a compilation of ultrasonic and Brillouin scattering data from the literature. In making the compilation, some scaling was applied to different data sets so that close overlap of C_{44} for the tetragonal structure was obtained (Fig. 8). This produced good agreement for the elastic constants of cubic $SrTiO_3$, C_{11}^0, C_{12}^0, C_{44}^0, but retained the wide scatter for C_{11} and C_{33} from twinned tetragonal crystals. Determination of values for the sixth order coefficients required some fitting to the data for C_{44}. On the other hand, the calculated variations of C_{11}, C_{33}, C_{12}, and C_{13} did not include any such reference to the experimental data. Agreement among calculated values of C_{11}, C_{33}, and C_{12} and experimental values obtained from individual twin domains of tetragonal crystals by Brillouin spectroscopy therefore implies a measure of success for Equation 29 in representing the real strain and elastic behavior of $SrTiO_3$. The additional anomalies in C_{44} and C_{66} below ~30 K are due to a different transition in ^{18}O-enriched samples.

Voigt/Reuss averages for the bulk and shear moduli of a polycrystalline sample have been calculated using Landau solutions for the individual elastic constants, and are shown in Figure 9a. Expressions for the Voigt limits are sufficiently simple to illustrate the influence of the coupling coefficients, λ_i, on the bulk elastic properties. For the *I*4/*mcm* structure these are

$$K_V = \frac{1}{3}\left(C_{11}^0 + 2C_{12}^0\right) - 4\lambda_1^2 \chi_1 q_1^2 \quad (41)$$

$$G_V = \frac{1}{5}\left(C_{11}^0 - C_{12}^0 + 3C_{44}^0\right) - \frac{2}{5}\left(8\lambda_2^2 \chi_1 + \lambda_3^2 \chi_3\right)q_1^2. \quad (42)$$

Values of the bulk modulus away from the transition point are hardly affected by the phase transition because coupling between the order parameter and volume strain is weak (λ_1 small). Softening of the shear modulus is greater owing to the stronger coupling between the order parameter and shear strains (larger values of λ_2, λ_3). This pattern of changes in K and G converts to sharp discontinuities in the velocities of P and S waves at the transition temperature, amounting to ~4% for V_p, and ~8% for V_s (Fig. 9b).

Some elastic softening occurs in the stability field of cubic $SrTiO_3$ as the transition point is approached from above. This is due to the effect of fluctuations, which are not included in the Landau free energy expansion. It is restricted to elastic constants,

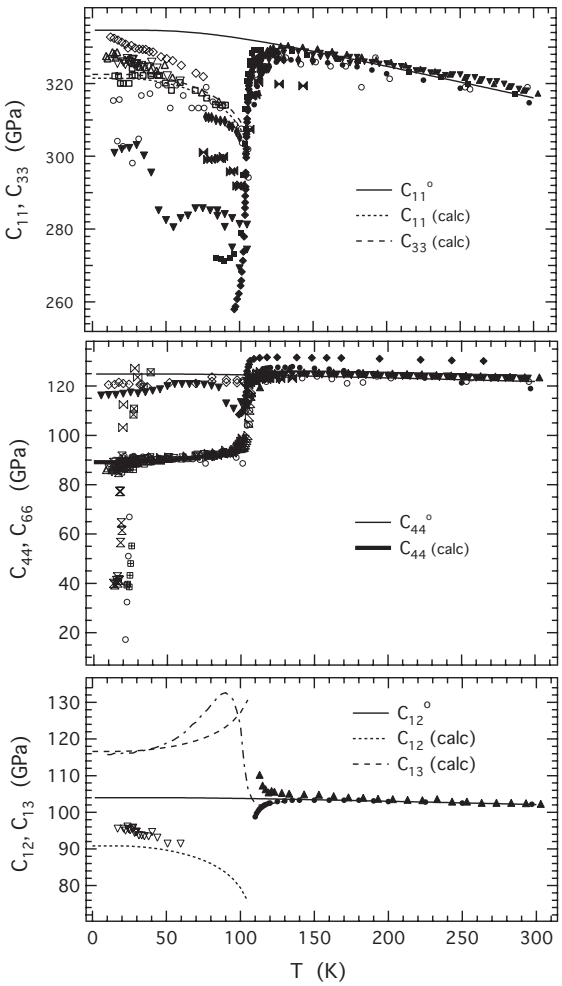

FIGURE 8. Compilation of elastic constant data from the literature (from Carpenter, in preparation). Filled symbols represent ultrasonic data; open symbols represent Brillouin scattering data. Lines are fits to the data for cubic $SrTiO_3$ (C_{11}^0, C_{12}^0, C_{44}^0) or calculated variations of elastic constants, with the exception of the dot-dash line, which is the experimental curve for a twinned crystal from Rehwald (1970). Data for C_{66} plot, as expected, close to the extrapolation of C_{44}^0 below 106 K. Additional softening of C_{44} and C_{66} below ~30 K is due to a different transition in ^{18}O-enriched samples.

which have the symmetry properties of the identity representation (i.e., $C_{11}^0 + 2\,C_{12}^0$ but not $C_{11}^0 - C_{12}^0$ or C_{44}^0). The softening, ΔC_{ik}, is described in general by a function of the form

$$\Delta C_{ik} = A_{ik}\left|T - T_c\right|^K \quad (43)$$

(as reviewed in Carpenter and Salje 1998), where A_{ik} and K are parameters obtained by fitting to experimental data. Softening of the bulk modulus just above T_c (Fig. 9a) derives from fits of Equation 43 to the experimental data for C_{11} and C_{12} above the transition temperature. The extent of this softening is probably exaggerated because of the influence of twin walls in the close vicinity of T_c and imprecise determinations of the exact transition point. Softening of G is due to an apparent softening of C_{44}, which, if real, must arise by some other mechanism.

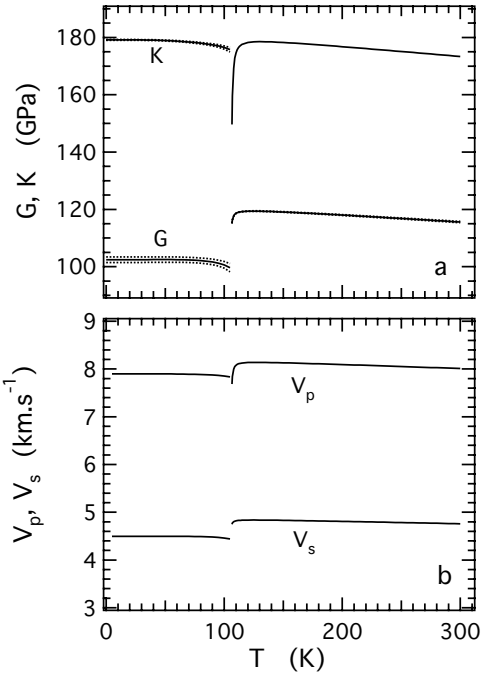

FIGURE 9. (**a**) Calculated variations of the bulk (*K*) and shear (*G*) moduli for a polycrystalline sample of $SrTiO_3$. Softening as $T \rightarrow T_c$ from above the transition point has been included, though calculated values are shown only down to T_c +1 K. Reuss and Voigt limits are shown as dotted lines. (**b**) Velocities of P and S waves calculated using the values of *K* and *G* in **a**, and a single (constant) value for density.

The elastic anomalies shown in Figure 9 do not represent the complete behavior of polycrystalline samples when the properties of ferroelastic twin walls are taken into account. At frequencies in the 1–300 Hz range, twinned tetragonal $SrTiO_3$ or $(Ca,Sr)TiO_3$ perovskite is much softer than could be expected from the Landau strain/order parameter coupling model (Kityk et al. 2000a, 2000b; Harrison et al. 2003). This is because proportions of an applied stress can be accommodated as strain due to displacements of the twin walls rather than simply by deformation of the crystal between twin walls. The effect involves dissipation of energy and is accompanied by a signature rise in attenuation. Similar softening is clearly present also at ultrasonic frequencies, as shown by the anomalously low values obtained for the average values of C_{11} and C_{33} obtained from tetragonal crystals (Fig. 8). This additional softening disappears once tetragonal crystals of $(Ca,Sr)TiO_3$ become orthorhombic (Harrison et al. 2003), however, implying that twin wall motion either cannot occur on the appropriate timescale or is otherwise impeded in the orthorhombic structure. The important implication of this for silicate perovskites is that a transition from orthorhombic to untwinned tetragonal crystals could result in a stiffening of bulk elastic properties, when the same transition to twinned crystals would give elastic softening. Tetragonal crystals of $CaSiO_3$, whether twinned or untwinned, would be expected to have significantly smaller seismic velocities than cubic $CaSiO_3$, due to a large change in shear modulus but little or no change in bulk modulus and density.

ELASTIC ANOMALIES ACCOMPANYING PROTON ORDERING AND DISPLACIVE COMPONENTS OF PHASE TRANSITIONS IN LAWSONITE, $CaAl_2Si_2O_7(OH)_2 \cdot 2H_2O$

Lawsonite is an unusual silicate mineral in that it has both a high density and a high water content (~11 wt% H_2O). These properties make it a potentially important phase with respect to the water budget during high-pressure, low-temperature metamorphism at subduction zones (Chatterjee et al. 1984; Pawley 1994; Schmidt and Poli 1994, 1998; Poli and Schmidt 1995; Schmidt 1995; Pawley et al. 1996; Holland et al. 1996; Grevel et al. 2000; Sinogeikin et al. 2000; Schilling et al. 2003). It has an orthorhombic framework structure with pairs of SiO_4 tetrahedra linked laterally by AlO_6 octahedra. Two types of channels parallel to the crystallographic x-axis contain protons belonging to OH groups, water molecules and calcium atoms (Fig. 10). In the present context lawsonite is of interest because it displays an unusual pattern of elastic constant variations associated with two low temperature phase transitions. These transitions were discovered by Libowitzky and Armbruster (1995) and Libowitzky and Rossman (1996), who showed that the symmetry changes, $Cmcm \leftrightarrow Pmcn$ at ~270 K and $Pmcn \leftrightarrow P2_1cn$ at ~150 K, can be understood in terms of changes in hydrogen bonding. The high-temperature transition is tricritical in character, while the low temperature transition is second order (Sondergeld et al. 2000a, 2000b, 2001; Meyer et al. 2000, 2001; Martín-Ollala et al. 2001; Carpenter et al. 2003).

Recent powder neutron diffraction studies have shown that proton ordering and framework distortions might contribute differently to the two phase transitions (Meyer et al. 2001; Carpenter et al. 2003). In particular, the transition temperature of the $Pmcn \leftrightarrow P2_1cn$ transition is 155 ± 1 K in a deuterated sample (~90% of H replaced by D) but 130 ± 1 K in a natural sample (Carpenter et al. 2003). This appears to be closely analogous with the ferroelectric phase transition in KH_2PO_4 (KDP) which

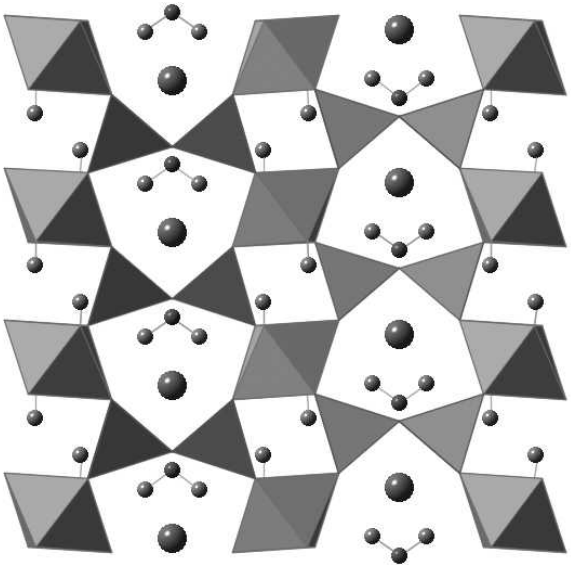

FIGURE 10. (100) plan view of the lawsonite structure. Channels parallel to [100] contain protons belonging to OH groups or H_2O molecules and calcium atoms.

is displaced from ~123 K to ~222 K by exchanging D for H (Samara 1973). Both transitions are ferroelectric and the properties of KDP are well known to be strongly influenced by the effects of proton ordering (e.g., Samara 1979, 1987). As in KDP, the symmetry-breaking mechanism in lawsonite presumably also depends on ordering of the protons (see, also, Sondergeld et al. 2001). In contrast, T_c = 271 ± 2 and 270 ± 1 K for the *Cmcm* ↔ *Pmcn* transition in D- and H-substituted lawsonite crystals, respectively. This implies, by reversal of the argument above, that proton ordering does not dominate in this transition. It appears that framework displacements, perhaps due to a soft optic mode, provide the symmetry-breaking mechanism. As with other phase transitions, the expectation is that variations of the elastic constants will provide indicative evidence of the underlying thermodynamic behavior.

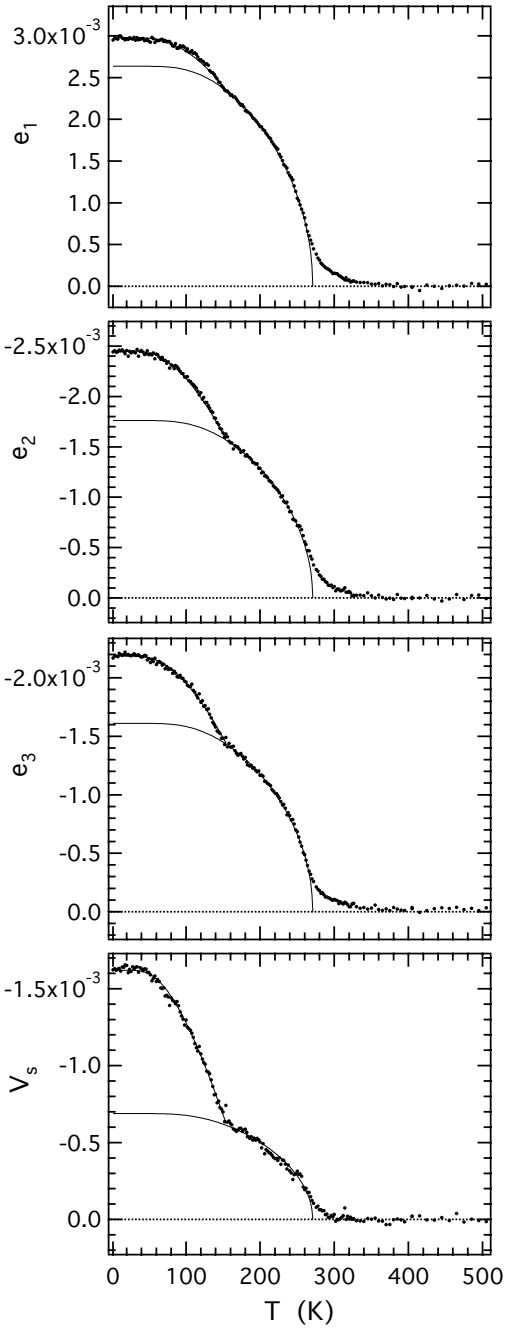

FIGURE 11. Spontaneous strain variations through the *Cmcm* ↔ *Pmcn* and *Pmcn* ↔ $P2_1cn$ transitions in deuterated lawsonite (after Carpenter et al. 2003). Curves through the data are tricritical fits for the *Cmcm* ↔ *Pmcn* transition and second order fits for the *Pmcn* ↔ $P2_1cn$ transition.

Elastic constant data are now available for the temperature range ~100–700 K (Schilling et al. 2003; Sondergeld et al. 2005), and can be used to test a simple model for the 270 K transition. A classical displacive transition giving a symmetry change *Cmcm* ↔ *Pmcn* would be expected to show patterns of strain and elastic constant variations determined by a standard Landau free energy expansion of the form (from Carpenter et al. 2003)

$$\begin{aligned} G = {} & \frac{1}{2}a\Theta_s\left[\coth\left(\frac{\Theta_s}{T}\right)-\coth\left(\frac{\Theta_s}{T_c}\right)\right]Q^2 \\ & +\frac{1}{4}bQ^4+\frac{1}{6}cQ^6+\lambda_1 e_1 Q^2+\lambda_2 e_2 Q^2 \\ & +\lambda_3 e_3 Q^2+\lambda_4 e_4^2 Q^2+\lambda_5 e_5^2 Q^2+\lambda_6 e_6^2 Q^2 \\ & +\frac{1}{2}\sum_{i,k} C_{ik}^0 e_i e_k . \end{aligned} \tag{44}$$

The same form of expansion should also apply to the *Pmcn* ↔ $P2_1cn$ transition. Spontaneous strain data for the deuterated sample are reproduced from Carpenter et al. (2003) in Figure 11. Each of the non-zero strains, e_1, e_2, e_3, V_s, is expected to vary linearly with Q^2 and their evolution with temperature is consistent with solutions to Equation 44 of the form (after Peréz-Mato and Salje 2000)

$$Q^n = 1-\frac{\coth\left(\Theta_s/T\right)}{\coth\left(\Theta_s/T_c\right)} \tag{45}$$

where n = 2 (second order) for the *Pmcn* ↔ $P2_1cn$ and n = 4 (tricritical) for the *Cmcm* ↔ *Pmcn* transition. In detail, there is an additional small anomaly which shows up in strain/strain plots (Fig. 12). This occurs at ~250 K in strain data from the deuterated sample but at ~225 K in the strain data from a natural sample (Carpenter et al. 2003). The displacement of ~25 K is identical to the displacement of T_c for the low temperature transition and implies that some additional structural changes associated with proton ordering develop well within the stability field of the *Pmcn* structure. The impact of this ordering on the absolute values of the spontaneous strains is small, but more substantial anomalies occur in other properties. For example, the frequencies of selected absorption bands in IR spectra collected below room temperature evolve as $(\Delta\omega)^2 \propto Q^4 \propto T$ but the band at ~3550 cm^{-1}, in particular, has a kink in the vicinity of 200 K (Meyer et al. 2000). The square of the average intensity of superlattice reflections from single crystal X-ray diffraction patterns also varies linearly with temperature ($I^2 \propto Q^4 \propto T_c - T$) but with a marked break in slope at ~222 K (Sondergeld et al. 2005).

Expressions for the elastic constant variations derived from Equation 44 (Carpenter et al. 2003) fall into two groups, depending on whether or not they contain the susceptibility, χ. C_{22}, C_{33}, C_{12}, C_{13}, and C_{23} have the same form as C_{11}, i.e.,

$$C_{11} = C_{11}^0 - 4\lambda_1^2 Q^2 \chi \quad (46)$$

where

$$\chi^{-1} = \frac{\partial^2 G}{\partial Q^2} = a\Theta_s \left[\coth\left(\frac{\Theta_s}{T}\right) - \coth\left(\frac{\Theta_s}{T_c}\right) \right] + \left(2b + b^*\right) Q^2 + 5cQ^4. \quad (47)$$

C_{55} and C_{66} have the same form as C_{44}, i.e.,

$$C_{44} = C_{44}^0 + 2\lambda_4 Q^2. \quad (48)$$

Values for the elastic constants of the high symmetry structure, C_{ik}^0, are given by the high temperature Brillouin scattering data of Schilling et al. (2003), while the variation of χ is known because values of the a, b, c coefficients are given by the heat capacity data of Martín-Olalla et al. (2001). Values of the coupling coefficients λ_1, λ_2, λ_3 have been extracted from the spontaneous strain data, so that the variations of C_{11}, C_{22}, and C_{33} can be calculated (Carpenter et al. 2003; Sondergeld et al. 2005). Experimental results obtained by ultrasonic methods at 15 MHz (Sondergeld et al. 2005) are compared with the calculated variations in Figure 13a. A purely displacive transition should cause softening as T decreases below T_c but this is only observed for a temperature interval of ~10 K. The most pronounced effects are substantial stiffening, demonstrating that Equation 44 is an inadequate model for the transition.

Data from Sondergeld et al. (2005) obtained at 13 MHz show that C_{44}, C_{55}, and C_{66} all stiffen with falling temperature below ~270 K (Fig. 13b). It has not been possible to estimate values for the coupling coefficients λ_4, λ_5 and λ_6, but ΔC_{44} (= $C_{44} - C_{44}^0$), ΔC_{55} (= $C_{55} - C_{55}^0$), ΔC_{66} (= $C_{66} - C_{66}^0$), should vary linearly with Q^2 (Eq. 48). For a tricritical transition, ΔC_{44}^2, ΔC_{55}^2, and ΔC_{66}^2 should all vary linearly with temperature, but, as seen in Figure 13c, this turns out to be approximately true only for ΔC_{66} when the data from Figure 13b are considered in this form. Differences of C_{44}, C_{55}, and C_{66} from the predicted behavior may be more revealing of the underlying mechanism of the phase transition than the differences of C_{11}, C_{22}, and C_{33},

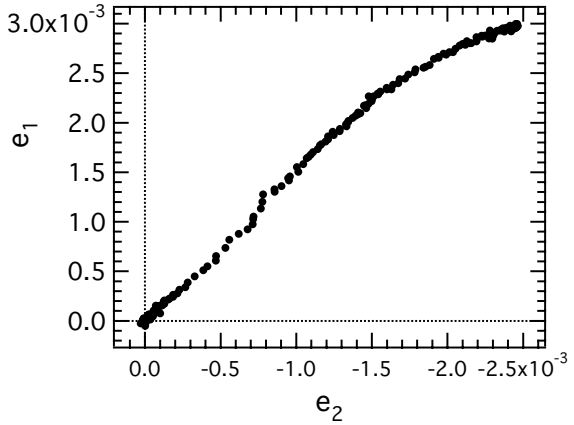

FIGURE 12. Strain/strain relationship for strains due to the phase transitions in deuterated lawsonite (after Carpenter et al. 2003). The kink at $e_1 \approx 1.2$, $e_2 \approx -0.8$ occurs at ~250 K. A similar kink is observed in all the strain data.

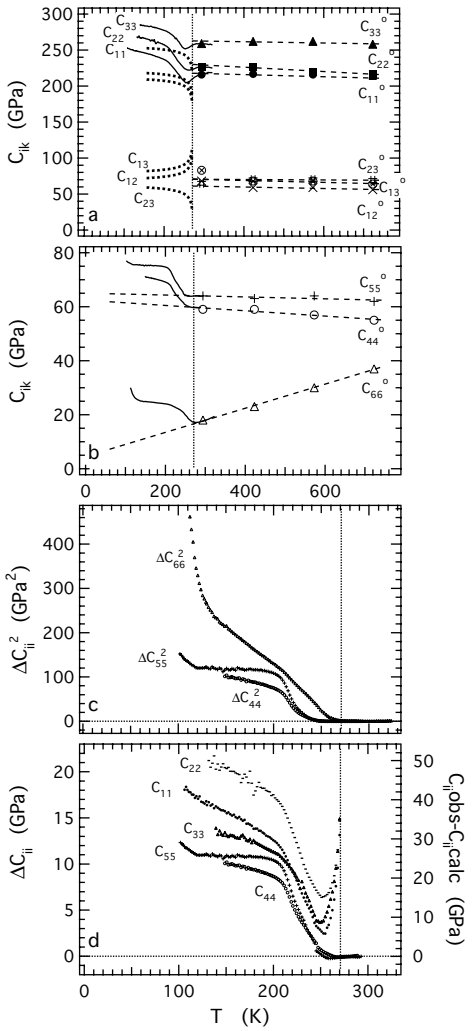

FIGURE 13. Elastic constants as a function of temperature for natural lawsonite. Data for four high temperatures from Schilling et al. (2003); low temperature data from Sondergeld et al. (2005). Note that Schilling et al. used reference axes for space group *Ccmm*. Their data have been relabeled for the axes of space group *Cmcm* used by Sondergeld et al. (2005). (**a**) Dashed lines are linear fits to the data of Schilling et al. (2003) to give values for C_{11}^0, C_{22}^0, and C_{33}^0. Dotted lines are calculated variations of C_{11}, C_{22}, C_{33}, C_{12}, C_{13}, C_{23} for a tricritical *Cmcm* ↔ *Pmcn* transition. Irregular curves are experimental data rescaled to produce a match with values of Schilling et al. at room temperature. (**b**) Broken lines representing C_{44}^0, C_{55}^0, and C_{66}^0 are fits to the data of Schilling et al. Irregular curves are experimental data of Sondergeld et al. rescaled so as to produce overlap with C_{44}^0, C_{55}^0, C_{66}^0 above room temperature. (**c**) ΔC_{44} is the difference between C_{44} and C_{44}^0 from **b** (and similarly for ΔC_{55}, ΔC_{66}). If the tricritical *Cmcm* ↔ *Pmcn* transition was driven by a single order parameter, each of ΔC_{44}^2, ΔC_{55}^2 and ΔC_{66}^2 would be expected to vary linearly with temperature. ΔC_{66}^2 shows a linear temperature-dependence over the stability range of the *Pmcn* structure, but with a distinct break in slope at ~210 K. ΔC_{44}^2 and ΔC_{55}^2 show a quite different evolution with temperature, suggesting that they couple with a second order parameter. (d) ΔC_{44}, ΔC_{55}, ΔC_{66} (left axis), as calculated for **c**. C_{11}obs – C_{11}calc is the difference between observed and calculated variations of C_{11} from **a**, and similarly for C_{22}, C_{33} (right axis). All five sets of data show the same general pattern of variation with temperature, marked by a distinct break in slope at ~210 K.

in that they reflect the variation of the order parameter without the need to have a model for the susceptibility. A minimum of two thermodynamic order parameters, Q_1 and Q_2, appears to be implicated. The first, Q_1, scales with the strain as $e_i \propto Q_1^2$, due to classical strain/order parameter coupling of the form $\lambda_i e_i Q_1^2$, and evolves with temperature as $Q_1^4 \propto T$. The evolution of ΔC_{66}^2 is then consistent with $\Delta C_{66} \propto Q_1^2$. The second order parameter behaves quite differently. It would contribute to a stiffening of all the elastic constants if it couples with strains as $\lambda_i e_i^2 Q_2^2$ and was not able to relax on the time scale of applied stresses during elastic constant measurements. In other words, it has the same characteristics as the order parameter for cation ordering discussed earlier for spinel and anorthite. In this case, the simplest model could have $\Delta C_{44} \propto \Delta C_{55} \propto Q_2^2$ and $\Delta C_{66} \propto Q_1^2$. Figure 13c is then a classical picture of bilinear order parameter coupling, closely resembling the behavior of Al/Si ordering and displacive components of the $C2/m \leftrightarrow C\bar{1}$ transition in albite (compare Fig. 13c with Fig. 10 of Salje et al. 1985). Symmetry is broken at $T = T_c$ by the development of Q_1 (ΔC_{66} increases). ΔC_{44} and ΔC_{55} ($\propto Q_2^2$) only increase slightly, however, suggesting that coupling between Q_1 and Q_2 is weak. ΔC_{44} and ΔC_{55} then increase sharply in a narrow temperature interval centered on ~225 K, before leveling off below ~200 K (Fig. 13c). The changes in curvature are mirrored by changes in curvature in ΔC_{66}^2, which can again be understood in terms of weak coupling between Q_1 and Q_2 (see Fig. 10 of Salje et al. 1985, for albite). In lawsonite, Q_2 is most probably associated with proton ordering and it is notable that the steep variation of ΔC_{55}, followed by a leveling off, is similar to the pattern of evolution of the order parameter in KDP (Fig. 8 of Hayward et al. 2001). Finally, if there are two such order parameters, the variations of C_{11}, C_{22}, and C_{33} should be due to a combination of softening due to the displacive process (Q_1) and stiffening due to proton ordering (Q_2). The difference among observed values of C_{11} and values calculated using Equation 46 should then scale with Q_2^2, and have the same pattern of evolution as ΔC_{44} and ΔC_{55}. Figure 13d shows that this appears to be more or less the case for each of C_{11}, C_{22}, and C_{33}.

Stiffening of the lawsonite structure due to proton ordering makes sense from a structural point of view. Hydrogen bonding in fixed orientations would effectively add mechanical braces across the channels of the structure (Fig. 10), making the whole framework less flexible. A complete model for the transition has not yet been developed but the expectation is that Q_1 will account predominantly for displacive effects while Q_2 describes proton ordering, as in KDP. However, changes in the 3600 cm^{-1} absorption band in IR spectra suggest that changes in hydrogen bonding start to occur at the transition temperature, and before the marked elastic stiffening sets in (Meyer et al. 2000). This reflects the tail in Q_2 above ~225 K or implies that Q_1 may have some component of dynamical ordering ahead of the large increase in Q_2. In either case, a configurational entropy term may be needed to give the correct evolution of Q_1 as $T \rightarrow 0$ K rather than a saturation temperature, Θ_s, for the displacive limit implied in Equation 44 (see, also, Hayward et al. 2002). The elastic constant data of Sondergeld et al. (2005) do not extend significantly into the $P2_1cn$ field but C_{11}, C_{55}, and C_{66}, at least, appear to show additional stiffening due to the $Pmcn \leftrightarrow P2_1cn$ transition. This is again consistent with the view that increased hydrogen bonding effectively braces the lawsonite structure.

The fact that displacive and proton ordering effects might be able to occur independently has interesting implications for the effects of pressure. Softening of C_{66} with falling temperature (Fig. 13b) would cause a proper ferroelastic transition to a monoclinic structure if C_{66} actually reached zero. This softening is reversed at the $Pmcn$ and $P2_1cn$ transitions, indicating that such a ferroelastic transition is suppressed by proton ordering. With increasing pressure at room temperature, both IR and Raman spectra show that some changes in hydrogen bonding occur (Scott and Williams, 1999; Daniel et al. 2000), but not to the same extent as is found at low temperatures. Instead, the monoclinic structure which would develop by softening of C_{66} appears above ~9.5 GPa (Daniel et al. 2000; Pawley and Allan 2001; Boffa Ballaran and Angel 2003). Daniel et al. did not observe any $h + k$ = odd reflections in single crystal diffraction patterns and suggested a symmetry change $Cmcm \leftrightarrow C2_1/m$. Boffa Ballaran and Angel (2003) found evidence for weak $h + k$ = odd reflections appearing at ~4 GPa, which would be consistent with a sequence $Cmcm \leftrightarrow Pmcn \leftrightarrow P2_1/m$. This is perhaps the same sequence as occurs at high temperatures in hennomartinite, which also has the lawsonite structure (Libowitzky and Armbruster 1996). In either case, elastic anomalies associated with the phase transitions due to increasing pressure should be more like those of classical displacive transitions. Differences in the response of the lawsonite structure to changes in pressure and temperature must imply that proton ordering and displacive effects couple differently with the volume strain. This should lead to a quite complex topology for the phase diagram at simultaneous high pressures and low temperatures. A stability field for the monoclinic structure at high pressures would be replaced by a stability field for the $P2_1cn$ structure at low temperatures. Between the two would be a stability field for the $Pmcn$ structure, but this could incorporate wide variations in the degree of proton order across it.

Concluding remarks

Three different mechanisms for modifying the elastic constants of minerals through the effects of cation ordering and displacive processes have been described. In general, cation ordering will cause changes to individual elastic constants that will scale either with Q^2 or Q, depending on whether the ordering is convergent or non-convergent. Crystals might get softer or stiffer due to the ordering. Elastic anomalies accompanying a displacive transition tend to involve softening because the transition, in effect, generates a new mechanism for a crystal to respond to external stress. The magnitude of these anomalies depends on the magnitude of the strain/order parameter coupling coefficients, while the pattern of changes depends on the thermodynamic character of the transition. Quite different and distinctive patterns develop at proper ferroelastic, improper ferroelastic or co-elastic transitions and depend also on whether a particular transition is second order, tricritical or first order. Transitions which involve both cation ordering and displacive processes, such as in lawsonite (or in albite and anorthite), will show combinations of these distinctive features. Non-convergent ordering can also influence displacive transitions, as in pigeonite (Cámara et al. 2002, 2003) and cummingtonite (Boffa Ballaran et al. 2000), and should lead to a further diversity of elastic constant

variations. The final mechanism of elastic softening, which has only been touched upon briefly in this paper, involves movement of ferroelastic twin walls. This mechanism is accompanied by characteristic attenuation effects and the softening is restricted to shear constants associated only with shear stresses that can cause the twin walls to move.

Because the pattern of elastic constant variations reflects the underlying mechanism of the processes responsible for them, it follows that displacive phase transitions in minerals at depth in the Earth's crust or mantle should give rise to distinctive seismic profiles. For quartz, the distinctive feature is a large change in P wave velocity (Fig. 1d). The proper ferroelastic transition in stishovite should cause a reduction of both P and S wave velocities as the transition is approached both from above and below (Fig. 6c). On the other hand, the improper ferroelastic transition in $SrTiO_3$ would give sharp discontinuities in both V_p and V_s (Fig. 9b), even in the absence of a significant density change. Cation ordering will modify the bulk elastic properties of minerals in the crust or mantle in more subtle ways, but the changes should conform to rather simple dependences on the order parameter.

Acknowledgments

Funding from the European Union (contract no. ERB-FMRX-CT-97-0108) and from the Natural Environment Research Council (grant no. NER/A/S2000/01055) is gratefully acknowledged. Reviewers are thanked for their reviews of the manuscript.

References cited

Agee, C.B. (1998) Phase transformations and seismic structure in the upper mantle and transition zone. In R.J. Hemley, Ed., Ultrahigh-Pressure Mineralogy: Physics and Chemistry of the Earth's Deep Interior, 37, p. 165–203. Reviews in Mineralogy, Mineralogical Society of America, Chantilly, Virginia.

Andrault, D., Fiquet, G., Guyot, F., and Hanfland, M. (1998) Pressure-induced Landau-type transition in stishovite. Science, 23, 720–724.

Andrault, D., Angel, R.J., Mosenfelder, J.L., and Le Bihan, T. (2003) Equation of state of stishovite to lower mantle pressures. American Mineralogist, 88, 301–307.

Andreozzi, G.B., Princivalle, F., Skogby, H., and Della Giusta, A. (2000) Cation ordering and structural variations with temperature in $MgAl_2O_4$ spinel: an X-ray single-crystal study. American Mineralogist, 85, 1164–1171.

Angel, R.J. (1988) High-pressure structure of anorthite. American Mineralogist, 73, 1114–1119.

——— (1992) Order-disorder and the high-pressure $P\bar{1}$-$I\bar{1}$ transition in anorthite. American Mineralogist, 77, 923–929.

——— (1994) Feldspars at high pressure. In I. Parsons, Ed., Feldspars and their reactions, NATO ASI series C, 421, 271–312. Kluwer, Dordrecht.

——— (2004) Equations of state of plagioclase feldspars. Contributions to Mineralogy and Petrology, 146, 506–512.

Angel, R.J., Hazen, R.M., McCormick, T.C., Prewitt, C.T., and Smyth, J.R. (1988) Comparative compressibility of end-member feldspars. Physics and Chemistry of Minerals, 15, 313–318.

Angel, R.J., Redfern, S.A.T., and Ross, N.L. (1989) Spontaneous strain below the $I\bar{1}$ - $P\bar{1}$ transition in anorthite at pressure. Physics and Chemistry of Minerals, 16, 539–544.

Angel, R.J., Carpenter, M.A., and Finger, L.W. (1990) Structural variation associated with compositional variation and order-disorder behaviour in anorthite-rich feldspars. American Mineralogist, 75, 150–162.

Askarpour, V., Manghnani, M.H., Fassbender, S., and Yoneda, A. (1993) Elasticity of single-crystal $MgAl_2O_4$ spinel up to 1273 K by Brillouin spectroscopy. Physics and Chemistry of Minerals, 19, 511–519.

Bärnighausen, H., Bossert, W., and Anselment, B. (1984) A second-order phase transition of calcium bromide and its geometrical interpretation. Acta Crystallographica A, 40, C96.

Bina, C.R. (1998) Lower mantle mineralogy and the geophysical perspective. In R.J. Hemley, Ed., Ultrahigh-Pressure Mineralogy: Physics and Chemistry of the Earth's Deep Interior, 37, p. 205–239. Reviews in Mineralogy, Mineralogical Society of America, Chantilly, Virginia.

Boffa Ballaran, T. and Angel, R.J. (2003) Equation of state and high-pressure phase transitions in lawsonite. European Journal of Mineralogy, 15, 241–246.

Boffa Ballaran, T., Angel, R.J., and Carpenter, M.A. (2000) High-pressure transformation behaviour of the cummingtonite-grunerite solid solution. European Journal of Mineralogy, 12, 1195–1213.

Bulou, A., Rousseau, M., and Nouet, J. (1992) Ferroelastic phase transitions and related phenomena. Key Engineering Materials, 68, 133–186.

Cámara, F., Carpenter, M.A., Domeneghetti, M.C., and Tazzoli, V. (2002) Non-convergent ordering and displacive phase transition in pigeonite: in situ HT XRD study. Physics and Chemistry of Minerals, 29, 331–340.

——— (2003) Coupling between non-convergent ordering and transition temperature in the $C2/c \leftrightarrow P2_1/c$ phase transition in pigeonite. American Mineralogist, 88, 1115–1128.

Caracas, R., Wentzcovitch, R., Price, G.D., and Brodholt, J. (2005) $CaSiO_3$ perovskite at lower mantle pressures. Geophysical Research Letters, 32, L06306, DOI:10.1029/2004GL022144.

Carbonin, S., Martignago, F., Menegazzo, G., and Dal Negro, A. (2002) X-ray single-crystal study of spinels: in situ heating. Physics and Chemistry of Minerals, 29, 503–514.

Carpenter, M.A. and Salje, E.K.H. (1994a) Thermodynamics of nonconvergent cation ordering in minerals: II. Spinels and the orthopyroxene solid solution. American Mineralogist, 79, 1068–1083.

——— (1994b) Thermodynamics of nonconvergent cation ordering in minerals: III. Order parameter coupling in potassium feldspar. American Mineralogist, 79, 1084–1098.

——— (1998) Elastic anomalies in minerals due to structural phase transitions. European Journal of Mineralogy, 10, 693–812.

Carpenter, M.A., McConnell, J.D.C., and Navrotsky, A. (1985) Enthalpies of ordering in the plagioclase feldspar solid solution. Geochimica et Cosmochimica Acta, 49, 947–966.

Carpenter, M.A., Angel, R.J., and Finger, L.W. (1990) Calibration of Al/Si order variations in anorthite. Contributions to Mineralogy and Petrology, 104, 471–480.

Carpenter, M.A., Powell, R., and Salje, E.K.H. (1994) Thermodynamics of non-convergent cation ordering in minerals: I. An alternative approach. American Mineralogist, 79, 1053–1067.

Carpenter, M.A., Salje, E.K.H., Graeme-Barber, A., Wruck, B., Dove, M.T., and Knight, K.S. (1998a) Calibration of excess thermodynamic properties and elastic constant variations associated with the $\alpha \leftrightarrow \beta$ phase transition in quartz. American Mineralogist, 83, 2–22.

Carpenter, M.A., Salje, E.K.H., and Graeme-Barber, A. (1998b) Spontaneous strain as a determinant of thermodynamic properties for phase transitions in minerals. European Journal of Mineralogy, 10, 621–691.

Carpenter, M.A., Hemley, R.J., and Mao, H.-K. (2000) High-pressure elasticity of stishovite and the $P4_2/mnm \leftrightarrow Pnnm$ phase transition. Journal of Geophysical Research, 105, 10807–10816.

Carpenter, M.A., Meyer, H.-W., Sondergeld, P., Marion, S., and Knight, K.S. (2003) Spontaneous strain variations through the low temperature phase transitions of deuterated lawsonite. American Mineralogist, 88, 534–546.

Chatterjee, N.D., Johannes, W., and Leistner, H. (1984) The system CaO-Al_2O_3-SiO_2-H_2O: new phase equilibria data, some calculated phase relations, and their petrological applications. Contributions to Mineralogy and Petrology, 88, 1–13.

Cohen, R.E. (1994) First-principles theory of crystalline SiO_2. In P.J. Heaney, C.T. Prewitt, and G.V. Gibbs, Eds., Silica: Physical Behavior, Geochemistry, and Materials Applications, 29, p. 369–402. Reviews in Mineralogy, Mineralogical Society of America, Chantilly, Virginia.

Cordier, P., Mainprice, D., and Mosenfelder, J.L. (2004) Mechanical instability near the stishovite–$CaCl_2$ phase transition: implications for crystal preferred orientations and seismic properties. European Journal of Mineralogy, 16, 387–399.

Cynn, H., Sharma, S.K., Cooney, T.F., and Nicol, M. (1992) High-temperature Raman investigation of order-disorder behavior in the $MgAl_2O_4$ spinel. Physical Review B, 45, 500–502.

Cynn, H., Anderson, O.L., and Nicol, M. (1993) Effects of cation disordering in a natural $MgAl_2O_4$ spinel observed by rectangular parallelepiped ultrasonic resonance and Raman measurements. Pure and Applied Geophysics, 141, 415–444.

Da Rocha, S. and Thibaudeau, P. (2003) Ab initio high-pressure thermodynamics of cationic disordered $MgAl_2O_4$ spinel. Journal of Physics: Condensed Matter, 15, 7103–7115.

Daniel, I., Fiquet, G., Gillet, P., Schmidt, M.W., and Hanfland, M. (2000) High-pressure behaviour of lawsonite: a phase transition at 8.6 GPa. European Journal of Mineralogy, 12, 721–733.

Della Giusta, A. and Ottonello, G. (1993) Energy and long-range disorder in simple spinels. Physics and Chemistry of Minerals, 20, 228–241.

Dubrovinsky, L.S. and Belonoshko, A.B. (1996) Pressure-induced phase transition and structural changes under deviatoric stress of stishovite to $CaCl_2$-like structure. Geochimica et Cosmochimica Acta, 60, 3657–3663.

Fiquet, G., Andrault, D., Dewaele, A., Charpin, T., Kunz, M., and Haüsermann, D. (1998) *P-V-T* equation of state of $MgSiO_3$ perovskite. Physics of the Earth and Planetary Interiors, 105, 21–31.

Fossheim, K. and Berre, B. (1972) Ultrasonic propagation, stress effects, and interaction parameters at the displacive transition in $SrTiO_3$. Physical Review

B, 5, 3292–3308.
Ghose, S., Van Tendeloo, G., and Amelinkx, S. (1988) Dynamics of a second-order phase transition: $P\bar{1}$ to $I\bar{1}$ phase transition in anorthite, $CaAl_2Si_2O_8$. Science, 242, 1539–1541.
Grevel, K.-D., Nowlan, E.U., Fasshauer, D.W., and Burchard, M. (2000) In situ X-ray diffraction investigation of lawsonite and zoisite at high pressures and temperatures. American Mineralogist, 85, 206–216.
Hackwell, T.P. and Angel, R.J. (1992) The comparative compressibility of reedmergnerite, danburite and their aluminium analogs. European Journal of Mineralogy, 4, 1221–1227.
Hahn, C. and Unruh, H.-G. (1991) Comment on "Temperature-induced structural phase transition in $CaBr_2$ studied by Raman-spectroscopy". Physical Review B, 12665–12667.
Haines, J. and Léger, J.M. (1993) Phase transitions in ruthenium dioxide up to 40 GPa: mechanism for the rutile-to-fluorite phase transformation and a model for the high-pressure behavior of stishovite SiO_2. Physical Review B, 48, 13344–13350.
——— (1997) X-ray diffraction study of the phase transitions and structural evolution of tin dioxide at high pressure: relationships between structure types and implications for other rutile-type dioxides. Physical Review B, 55, 11144–11154.
Haines, J., Léger, J.M., and Hoyau, S. (1995) Second-order rutile-type to $CaCl_2$-type phase transition in β-MnO_2 at high pressure. Journal of Physics and Chemistry of Solids, 56, 965–973.
Haines, J., Léger, J.M., and Schulte, O. (1996) The high-pressure phase transition sequence from rutile-type through to the cotunnite-type structure in PbO_2. Journal of Physics: Condensed Matter, 8, 1631–1646.
Haines, J., Léger, J.M., Schulte, O., and Hull, S. (1997) Neutron diffraction study of the ambient-pressure, rutile-type and the high-pressure, $CaCl_2$-type phases of ruthenium dioxide. Acta Crystallographica B, 53, 880–884.
Haines, J., Léger, J.M., Chateau, C., Bini, R., and Ulivi, L. (1998) Ferroelastic phase transition in rutile-type germanium dioxide at high pressure. Physical Review B, 58, R2909–R2912.
Haines, J., Léger, J.M., Chateau, C., and Pereira, A.S. (2000) Structural evolution of rutile-type and $CaCl_2$-type germanium dioxide at high pressures. Physics and Chemistry of Minerals, 27, 575–582.
Haines, J., Léger, J.M., Gorelli, F., Klug, D.D., Tse, J.S., and Li, Z.Q. (2001) X-ray diffraction and theoretical studies of the high-pressure structures and phase transitions in magnesium fluoride. Physical Review B, 64, 134110.
Harrison, R.J. and Redfern, S.A.T. (2002) The influence of transformation twins on the seismic-frequency elastic and anelastic properties of perovskite: dynamical mechanical analysis of single crystal $LaAlO_3$. Physics of the Earth and Planetary Interiors, 134, 253–272.
Harrison, R.J., Redfern, S.A.T., and Smith, R.I. (2000) In-situ study of the $R\bar{3}$ to *R3c* phase transition in the ilmenite-hematite solid solution using time-of-flight neutron powder diffraction. American Mineralogist, 85, 194–205.
Harrison. R.J., Redfern, S.A.T., and Street, J. (2003) The effect of transformation twins on the seismic-frequency mechanical properties of polycrystalline $Ca_{1-x}Sr_xTiO_3$ perovskite. American Mineralogist, 88, 574–582.
Harrison, R.J., Redfern, S.A.T., Buckley, A., and Salje, E.K.H. (2004a) Application of real-time, stroboscopic x-ray diffraction with dynamical mechanical analysis to characterize the motion of ferroelastic domain walls. Journal of Applied Physics, 95, 1706–1717.
Harrison, R.J., Redfern, S.A.T., and Salje, E.K.H. (2004b) Dynamical excitation and anelastic relaxation of ferroelastic domain walls in $LaAlO_3$. Physical Review B, 69, 144101.
Harrison, R.J., Redfern, S.A.T., and Bismayer, U. (2004c) Seismic-frequency attenuation at first-order phase transitions: dynamical mechanical analysis of pure and Ca-doped lead orthophosphate. Mineralogical Magazine, 68, 839–852.
Hawthorne, F.C., Ungaretti, L., Oberti, R., Caucia, F., and Callegari, A. (1993) The crystal-chemistry of staurolite. II. Order-disorder and the monoclinic → orthorhombic phase transition. Canadian Mineralogist, 31, 583–595.
Hayward, S.A. and Salje, E.K.H. (1999) Cubic-tetragonal phase transition in $SrTiO_3$ revisited: Landau theory and transition mechanism. Phase Transitions, 68, 501–522.
Hayward, S.A., Gallardo, M.C., and Salje, E.K.H. (2001) Ferroelectric phase transition in DKDP: a macroscopic order-disorder model. Ferroelectrics, 255, 123–137.
Hayward, S.A., Burriel, R., Marion, S., Meyer, H.-W., and Carpenter, M.A. (2002) Kinetic effects associated with the low-temperature phase transitions in lawsonite. European Journal of Mineralogy, 14, 1145–1153.
Hazen, R.M. and Yang, H. (1999) Effects of cation substitution and order-disorder on *P-V-T* equations of state of cubic spinels. American Mineralogist, 84, 1956–1960.
Hellwig, H., Goncharov, A.F., Gregoryanz, E., Mao, H.-K., and Hemley, R.J. (2003) Brillouin and Raman spectroscopy of the ferroelastic rutile-to-$CaCl_2$ transition in SnO_2 at high pressure. Physical Review B, 67, 174110.
Hemley, R.J., Prewitt, C.T., and Kingma, K.J. (1994) High-pressure behavior of silica. In P.J. Heaney, C.T. Prewitt, and G.V. Gibbs, Eds., Silica: Physical Behavior, Geochemistry, and Materials Applications, 29, p. 41–81. Reviews in Mineralogy, Mineralogical Society of America, Chantilly, Virginia.
Hemley, R.J., Shu, J., Carpenter, M.A., Hu, J., Mao, H.K, and Kingma, K.J. (2000) Strain/order parameter coupling in the ferroelastic transition in dense SiO_2. Solid State Communications, 114, 527–532.
Holland, T.J.B., Redfern, S.A.T., and Pawley, A.R. (1996) Volume behavior of hydrous minerals at high pressure and temperature: II. Compressibilities of lawsonite, zoisite, clinozoisite and epidote. American Mineralogist, 81, 341–348.
Karki, B.B., Stixrude, L., and Crain, J. (1997a) Ab initio elasticity of three high-pressure polymorphs of silica. Geophysical Research Letters, 24, 3269–3272.
Karki, B.B., Warren, M.C., Stixrude, L., Ackland, G.J., and Crain, J. (1997b) Ab initio studies of high-pressure structural transformations in silica. Physical Review B, 55, 3465–3471.
Kennedy, B.J. and Howard, C.J. (2004) Synchrotron x-ray powder diffraction study of the structural phase transition in $CaBr_2$. Physical Review B, 70, 144102.
Kingma, K.J., Cohen, R.E., Hemley, R.J., and Mao, H.-K. (1995) Transformation of stishovite to a denser phase at lower-mantle pressures. Nature, 374, 243–245.
Kityk, A.V., Schranz, W., Sondergeld, P., Havlik, D., Salje, E.K.H., and Scott, J.F. (2000a) Low-frequency superelasticity and nonlinear elastic behavior of $SrTiO_3$ crystals. Physical Review B, 61, 946–956.
Kityk, A.V., Schranz, W., Sondergeld, P., Havlik, D., Salje, E.K.H., and Scott, J.F. (2000b) Nonlinear elastic behaviour of $SrTiO_3$ crystals in the quantum paraelectric regime. Europhysics Letters, 50, 41–47.
Kurashina, T., Hirose, K., Ono, S., Sata, N., and Ohishi, Y. (2004) Phase transition in Al-bearing $CaSiO_3$ perovskite: implications for seismic discontinuities in the lower mantle. Physics of the Earth and Planetary Interiors, 145, 67–74.
Lavrentiev, M.Y., Purton, J.A., and Allan, N.L. (2003) Ordering in spinels—a Monte Carlo study. American Mineralogist, 88, 1522–1531.
Lee, C. and Gonze, X. (1995) The pressure-induced ferroelastic phase transition of SiO_2 stishovite. Journal of Physics: Condensed Matter, 7, 3693–3698.
——— (1997) SiO_2 stishovite under high pressure: dielectric and dynamical properties and the ferroelastic phase transition. Physical Review B, 56, 7321–7330.
Li, B., Rigden, S.M., and Liebermann, R.C. (1996) Elasticity of stishovite at high pressure. Physics of the Earth and Planetary Interiors, 96, 113–127.
Libowitzky, E. and Armbruster, T. (1995) Low-temperature phase transitions and the role of hydrogen bonds in lawsonite. American Mineralogist, 80, 1277–1285.
——— (1996) Lawsonite-type phase transitions in hennomartinite, $SrMn_2(Si_2O_7)(OH)_2.H_2O$. American Mineralogist, 81, 9–18.
Libowitzky, E. and Rossman, G.R. (1996) FTIR spectroscopy of lawsonite between 82 and 325 K. American Mineralogist, 81, 1080–1091.
Liu, M., Finlayson, T.R., and Smith, T.F. (1997) High-resolution dilatometry measurements of $SrTiO_3$ along cubic and tetragonal axes. Physical Review B, 55, 3480–3484.
Lodziana, Z., Parlinski, K., and Hafner, J. (2001) Ab initio studies of high-pressure transformations in GeO_2. Physical Review B, 63, 134106.
Lüthi, B. and Moran, T.J. (1970) Sound propagation near the structural phase transition in strontium titanate. Physical Review B, 2, 1211–1214.
Maekawa, H., Kato, S., Kawamura, K., and Yokokawa, T. (1997) Cation mixing in natural $MgAl_2O_4$ spinel: a high-temperature ^{27}Al NMR study. American Mineralogist, 82, 1125–1132.
Mao, H.K., Shu, J., Hu, J., and Hemley, R.J. (1994) Single-crystal X-ray diffraction of stishovite to 65 GPa. Eos Transactions of the American Geophysical Union, 75, 662.
Martín-Olalla, J.-M., Hayward, S.A., Meyer, H.-W., Ramos, S., del Cerro, J., and Carpenter, M.A. (2001) Phase transitions in lawsonite: a calorimetric study. European Journal of Mineralogy, 13, 5–14.
Mechie, J., Sobolev, S.V., Ratschbacher, L., Babeyko, A.Y., Bock, G., Jones, A.G., Nelson, K.D., Solon, K.D., Brown, L.D., and Zhao, W. (2004) Precise temperature estimation in the Tibetan crust from seismic detection of the α-β quartz transition. Geology, 32, 601–604.
Méducin, F., Redfern, S.A.T., Le Godec, Y., Stone, H.J., Tucker, M.G., Dove, M.T., and Marshall, W.G. (2004) Study of cation order-disorder in $MgAl_2O_4$ spinel by in situ neutron diffraction up to 1600 K and 3.2 GPa. American Mineralogist, 89, 981–986.
Meyer, H.-W., Carpenter, M.A., Graeme-Barber, A., Sondergeld, P., and Schranz, W. (2000) Local and macroscopic order parameter variations associated with low temperature phase transitions in lawsonite, $CaAl_2Si_2O_7(OH)_2.H_2O$. European Journal of Mineralogy, 12, 1139–1150.
Meyer, H.-W., Marion, S., Sondergeld, P., Carpenter, M.A., Knight, K.S., Redfern, S.A.T., and Dove, M.T. (2001) Displacive components of the low-temperature phase transitions in lawsonite. American Mineralogist, 86, 566–577.
Millard, R.L., Peterson, R.C., and Hunter, B.K. (1992) Temperature dependence of cation disorder in $MgAl_2O_4$ spinel using ^{27}Al and ^{17}O magic-angle spinning NMR. American Mineralogist, 77, 44–52.
Navrotsky, A. (1986) Cation-distribution energetics and heats of mixing in

$MgFe_2O_4$-$MgAl_2O_4$, $ZnFe_2O_4$-$ZnAl_2O_4$, and $NiAl_2O_4$-$ZnAl_2O_4$ spinels: study by high-temperature calorimetry. American Mineralogist, 71, 1160–1169.

Navrotsky, A. and Kleppa, O.J. (1967) The thermodynamics of cation distributions in simple spinels. Journal of Inorganic and Nuclear Chemistry, 29, 2701–2714.

Navrotsky, A., Wechsler, B.A., Geisinger, K., and Seifert, F. (1986) Thermochemistry of $MgAl_2O_4$-$Al_{8/3}O_4$ defect spinels. Journal of the American Ceramic Society, 69, 418–422.

Okazaki, A. and Kawaminami, M. (1973) Lattice constant of strontium titanate at low temperatures. Materials Research Bulletin, 8, 545–550.

O'Neill, H.St.C. and Navrotsky, A. (1983) Simple spinels: crystallographic parameters, cation radii, lattice energies, and cation distribution. American Mineralogist, 68, 181–194.

Ono, S., Hirose, K., Murakami, M., and Isshiki, M. (2002a) Post-stishovite phase boundary in SiO_2 determined by in situ X-ray observations. Earth and Planetary Science Letters, 197, 187–192.

——— (2002b) Phase boundary between rutile-type and $CaCl_2$-type germanium dioxide determined by in situ X-ray observations. American Mineralogist, 87, 99–102.

Ono, S., Kikegawa, T., and Iizuka, T. (2004a) The equation of state of orthorhombic perovskite in a peridotitic mantle composition to 80 GPa: implications for chemical composition of the lower mantle. Physics of the Earth and Planetary Interiors, 145, 9–17.

Ono, S., Ohishi, Y., and Mibe, K. (2004b) Phase transition of Ca-perovskite and stability of Al-bearing Mg-perovskite in the lower mantle. American Mineralogist, 89, 1480–1485.

Parlinski, K. and Kawazoe, Y. (2000) Ab initio study of phonons in the rutile structure of SnO_2 under pressure. European Physical Journal B, 13, 679–683.

Pavese, A., Artioli, G., and Hull, S. (1999) In situ powder neutron diffraction of cation partitioning vs. pressure in $Mg_{0.94}Al_{2.04}O_4$ synthetic spinel. American Mineralogist, 84, 905–912.

Pawley, A.R. (1994) The pressure and temperature stability limits of lawsonite: implications for H_2O recycling in subduction zones. Contributions to Mineralogy and Petrology, 118, 99–108.

Pawley, A.R. and Allan, D.R. (2001) A high-pressure structural study of lawsonite using angle-dispersive powder-diffraction methods with synchrotron radiation. Mineralogical Magazine, 65, 41–58.

Pawley, A.R., Redfern, S.A.T., and Holland, T.J.B. (1996) Volume behavior of hydrous minerals at high pressures and temperatures: I. Thermal expansion of lawsonite, zoisite, clinozoisite, and diaspore. American Mineralogist, 81, 335–340.

Pérez-Mato, J.M. and Salje, E.K.H. (2000) Quantum fluctuations of order parameters in structural phase transitions and the pressure dependence of transition temperatures. Journal of Physics: Condensed Matter, 12, L29–L34.

Peterson, R.C., Lager, G.A., and Hitterman, R.L. (1991) A time-of-flight neutron powder diffraction study of $MgAl_2O_4$ at temperatures up to 1273 K. American Mineralogist, 76, 1455–1458.

Poli, S. and Schmidt, M.W. (1995) H_2O transport and release in subduction zones: experimental constraints on basaltic and andesitic systems. Journal of Geophysical Research, 100, 22299–22314.

Prewitt, C.T. and Downs, R.T. (1998) High-pressure crystal chemistry. In R.J. Hemley, Ed., Ultrahigh-Pressure Mineralogy: Physics and Chemistry of the Earth's Deep Interior, 37, p. 283–317. Reviews in Mineralogy, Mineralogical Society of America, Chantilly, Virginia.

Putnis, A., Salje, E., Redfern, S.A.T., Fyfe, C.A., and Strobl, H. (1987) Structural states of Mg-cordierite I: order parameters from synchrotron X-ray and NMR data. Physics and Chemistry of Minerals, 14, 446–454.

Raptis, C., McGreevy, R.L., and Seguier, D.G. (1989) Temperature-induced structural phase transition in $CaBr_2$ studied by Raman spectroscopy. Physical Review B, 7996–7999.

Redfern, S.A.T. (1992) The effect of Al/Si disorder on the $I\bar{1}$ - $P\bar{1}$ co-elastic phase transition in Ca-rich plagioclase. Physics and Chemistry of Minerals, 19, 246–254.

Redfern, S.A.T. and Salje, E. (1987) Thermodynamics of plagioclase II: temperature evolution of the spontaneous strain at the $I\bar{1} \leftrightarrow P\bar{1}$ phase transition in anorthite. Physics and Chemistry of Minerals, 14, 189–195.

——— (1992) Microscopic dynamic and macroscopic thermodynamic character of the $I\bar{1}$-$P\bar{1}$ phase transition in anorthite. Physics and Chemistry of Minerals, 18, 526–533.

Redfern, S.A.T., Graeme-Barber, A., and Salje, E. (1988) Thermodynamics of plagioclase III: spontaneous strain at the $I\bar{1}$-$P\bar{1}$ phase transition in Ca-rich plagioclase. Physics and Chemistry of Minerals, 16, 157–163.

Redfern, S.A.T., Harrison, R.J., O'Neill, H.St.C., and Wood, D.R.R. (1999) Thermodynamics and kinetics of cation ordering in $MgAl_2O_4$ spinel up to 1600 °C from in situ neutron diffraction. American Mineralogist, 84, 299–310.

Rehwald, W. (1970) Low temperature elastic moduli of strontium titanate. Solid State Communications, 8, 1483–1485.

——— (1971) Ultrasonic properties of strontium titanate at the 105° K transition. Physik der Kondensierten Materie, 14, 21–36.

Ross, N.L., Shu, J.F., Hazen, R.M., and Gasparik, T. (1990) High-pressure crystal chemistry of stishovite. American Mineralogist, 75, 739–747.

Sack, R.O. and Ghiorso, M.S. (1991) An internally consistent model for the thermodynamic properties of Fe-Mg-titanomagnetite-aluminate spinels. Contributions to Mineralogy and Petrology, 106, 474–505.

Salje, E. (1987) Thermodynamics of plagioclases I: theory of the $I\bar{1}$-$P\bar{1}$ phase transition in anorthite and Ca-rich plagioclases. Physics and Chemistry of Minerals, 14, 181–188.

Salje, E., Kuscholke, B., Wruck, B., and Kroll, H. (1985) Thermodynamics of sodium feldspar II: experimental results and numerical calculations. Physics and Chemistry of Minerals, 12, 99–107.

Salje, E.K.H., Wruck, B., and Thomas, H. (1991a) Order-parameter saturation and low-temperature extension of Landau theory. Zeitschrift für Physik B: Condensed Matter, 82, 399–404.

Salje, E.K.H., Wruck, B., and Marais, S. (1991b) Order parameter saturation at low temperatures—numerical results for displacive and o/d systems. Ferroelectrics, 124, 185–188.

Samara, G.A. (1973) The effects of deuteration on the static ferroelectric properties of KH_2PO_4 (KDP). Ferroelectrics, 5, 25–37.

——— (1979) Pressure dependence of the static dielectric properties of $K(H_{1-x}D_x)_2PO_4$ and RbH_2PO_4. Ferroelectrics, 22, 925–936.

——— (1987) Pressure dependence of the static and dynamic properties of KH_2PO_4 and related ferroelectric and antiferroelectric crystals. Ferroelectrics, 71, 161–182.

Schilling, F.R., Sinogeikin, S.V., and Bass, J.D. (2003) Single-crystal elastic properties of lawsonite and their variations with temperature. Physics of Earth and Planetary Interiors, 136, 107–118.

Schmidt, M.W. (1995) Lawsonite: upper pressure stability and formation of higher density hydrous phases. American Mineralogist, 80, 1286–1292.

Schmidt, M.W. and Poli, S. (1994) The stability of lawsonite and zoisite at high pressures: experiments in CASH to 92 kbar and implications for the presence of hydrous phases in subducted lithosphere. Earth and Planetary Science Letters, 124, 105–118.

——— (1998) Experimentally based water budgets for dehydrating slabs and consequences for arc magma generation. Earth and Planetary Science Letters, 163, 361–379.

Schmocker, U. and Waldner, F. (1976) The inversion parameter with respect to the space group of $MgAl_2O_4$ spinels. Journal of Physics C: Solid State Physics, 9, L235–237.

Scott, H.P. and Williams, Q. (1999) An infrared spectroscopic study of lawsonite to 20 GPa. Physics and Chemistry of Minerals, 26, 437–445.

Shieh, S.R., Duffy, T.S., and Li, B. (2002) Strength and elasticity of SiO_2 across the stishovite–$CaCl_2$-type structural phase boundary. Physical Review Letters, 89, 255507.

Sinogeikin, S.V., Schilling, F.R., and Bass, J.R. (2000) Single crystal elasticity of lawsonite. American Mineralogist, 85, 1834–1837.

Slonczewski, J.C. and Thomas, H. (1970) Interaction of elastic strain with the structural transition of strontium titanate. Physical Review B, 1, 3599–3608.

Smith, J.V. and Brown, W.L. (1988) Feldspar minerals. Crystal structures, physical, chemical, and microstructural properties, vol. 1. Springer-Verlag, New York.

Sondergeld, P., Schranz, W., Kityk, A.V., Carpenter, M.A., and Libowitzky, E. (2000a) Ordering behaviour of the mineral lawsonite. Phase Transitions, 71, 189–203.

Sondergeld, P., Schranz, W., Tröster, A., Carpenter, M.A., Libowitzky, E., and Kityk, A.V. (2000b) Optical, elastic, and dielectric studies of the phase transitions in lawsonite. Physical Review B, 62, 6143–6147.

Sondergeld, P., Schranz, W., Tröster, A., Kabelka, H., Meyer, H.-W., Carpenter, M.A., Lodziana, Z., and Kityk, A.V. (2001) Dielectric relaxation and order-parameter dynamics in lawsonite. Physical Review B, 64, 024105.

Sondergeld, P., Schranz, W., Tröster, A., Armbruster, T., Giester, G., Kityk, A., and Carpenter, M.A. (2005) Ordering and elasticity associated with low-temperature phase transitions in lawsonite. American Mineralogist, 90, 448–456.

Stixrude, L. and Cohen, R.E. (1993) Stability of orthorhombic $MgSiO_3$ perovskite in the Earth's lower mantle. Nature, 364, 613–615.

Stixrude, L., Cohen, R.E., Yu, R., and Krakauer, H. (1996) Prediction of phase transition in $CaSiO_3$ perovskite and implications for lower mantle structure. American Mineralogist, 81, 1293–1296.

Suzuki, I., Ohno, I., and Anderson, O.L. (2000) Harmonic and anharmonic properties of spinel $MgAl_2O_4$. American Mineralogist, 85, 304–311.

Teter, D.M., Hemley, R.J., Kresse, G., and Hafner, J. (1998) High pressure polymorphism in silica. Physical Review Letters, 80, 2145–2148.

Tröster, A., Schranz, W., and Miletich, R. (2002) How to couple Landau theory to an equation of state. Physical Review Letters, 88, 055503.

Tsuchiya, T., Caracas, R., and Tsuchiya, J. (2004) First principles determination of the phase boundary of high-pressure polymorphs of silica. Geophysical Research Letters, 31, L11610, DOI:10.1029/2004GL019649.

Unruh, H.-G. (1993) Ferroelastic phase transitions in calcium chloride and calcium bromide. Phase Transitions, 45, 77–89.

Van Minh, N. and Yang, I.-S. (2004) A Raman study of cation-disorder transi-

tion temperature of natural $MgAl_2O_4$ spinel. Vibrational Spectroscopy, 35, 93–96.

Van Tendeloo, G., Ghose, S., and Amelinckx, S. (1989) A dynamical model for the $P\bar{1}$ - $I\bar{1}$ phase transition in anorthite, $CaAl_2Si_2O_8$ I. Evidence from electron microscopy. Physics and Chemistry of Minerals, 16, 311–319.

Warren, M.C., Dove, M.T., and Redfern, S.A.T. (2000a) Disordering of $MgAl_2O_4$ spinel from first principles. Mineralogical Magazine, 64, 311–317.

——— (2000b) Ab initio simulations of cation ordering in oxides: application to spinel. Journal of Physics: Condensed Matter, 12, L43–L48.

Watt, J.P. (1979) Hashin-Shtrikman bounds on the effective elastic moduli of polycrystals with orthorhombic symmetry. Journal of Applied Physics, 50, 6290–6295.

Watt, J.P. and Peselnik. L. (1980) Clarification of the Hashin-Shtrikman bounds on the effective elastic moduli of polycrystals with hexagonal, trigonal, and tetragonal symmetries. Journal of Applied Physics, 51, 1525–1531.

Wentzcovitch, R.M., Martins, J.L., and Price, G.D. (1993) Ab initio molecular dynamics with variable cell shape: application to $MgSiO_3$. Physical Review Letters, 70, 3947–3950.

Wood, B.J., Kirkpatrick, R.J., and Montez, B. (1986) Order-disorder phenomena in $MgAl_2O_4$ spinel. American Mineralogist, 71, 999–1006.

Yamanaka, T. and Takéuchi, Y. (1983) Order-disorder transition in $MgAl_2O_4$ spinel at high temperatures up to 1700 °C. Zeitschrift für Kristallographie, 165, 65–78.

MANUSCRIPT RECEIVED MAY 9, 2005
MANUSCRIPT ACCEPTED OCTOBER 12, 2005
MANUSCRIPT HANDLED BY DAN SHIM